Methods for determining key components in a mathematical model for tumor–immune dynamics in multiple myeloma

Jill Gallaher [a], Kamila Larripa [b], Marissa Renardy [c,d], Blerta Shtylla [e], Nessy Tania [f], Diana White [g], Karen Wood [h,i], Li Zhu [j], Chaitali Passey [j,k], Michael Robbins [l], Natalie Bezman [m], Suresh Shelat [n], Hearn Jay Cho [o,1], Helen Moore [p,q,1,*]

[a] H. Lee Moffitt Cancer Center, Tampa, FL 33612, USA
[b] Department of Mathematics, Humboldt State University, Arcata, CA 95521, USA
[c] Department of Mathematics, The Ohio State University, Columbus, OH 43210, USA
[d] Current affiliation: Department of Microbiology and Immunology, University of Michigan, Ann Arbor, MI 48109, USA
[e] Mathematics Department, Pomona College, Claremont, CA 91711, USA
[f] Department of Mathematics and Statistics, Smith College, Northampton, MA 01063,USA
[g] Department of Mathematics, Clarkson University, Potsdam, NY 13699, USA
[h] Department of Mathematics, University of California at Irvine, Irvine, CA 92697, USA
[i] Current affiliation: The Aerospace Corporation, El Segundo, CA 90245, USA
[j] Clinical Pharmacology and Pharmacometrics, Bristol-Myers Squibb, Princeton, NJ 08543, USA
[k] Current affiliation: Genmab, Monmouth Junction, NJ 08852, USA
[l] Hematology Medical Strategy, Bristol-Myers Squibb, Lawrence Township, NJ 08648, USA
[m] Immuno-Oncology Discovery, Bristol-Myers Squibb, Redwood City, CA 94063, USA
[n] Oncology Clinical Development, Bristol-Myers Squibb, Lawrence Township, NJ 08648, USA
[o] Tisch Cancer Institute, Mt. Sinai School of Medicine, New York, NY 10029, USA
[p] Bristol-Myers Squibb, Princeton, NJ 08543, USA
[q] Current affiliation: AstraZeneca, Waltham, MA 02451, USA

ARTICLE INFO

ABSTRACT

In this work, we analyze a mathematical model we introduced previously for the dynamics of multiple myeloma and the immune system. We focus on four main aspects: (1) obtaining and justifying ranges and values for all parameters in the model; (2) determining a subset of parameters to which the model is most sensitive; (3) determining which parameters in this subset can be uniquely estimated given certain types of data; and (4) exploring the model numerically. Using global sensitivity analysis techniques, we found that the model is most sensitive to certain growth, loss, and efficacy parameters. This analysis provides the foundation for a future application of the model: prediction of optimal combination regimens in patients with multiple myeloma.

1. Introduction

Multiple myeloma (MM) is a cancer of plasma B cells. Although there are almost two dozen treatments approved in the US and others currently in clinical trials, many patients do not survive more than ten years (Kazandjian and Landgren, 2016). Regimens usually combine multiple therapies (two, three, or more drugs) simultaneously. Patients receive additional combination therapies if they do not respond to the initial combination, or when they relapse. Without direct comparison studies, it is difficult to know the best combinations and doses for treatment, and questions remain regarding both treatment choice and timing (Kazandjian and Landgren, 2016). A mathematical model that accurately captures

important features of the disease and therapy dynamics can be used to test regimens in silico. It can also be used to calculate a regimen that is predicted to perform optimally.

A number of mathematical models for the progression of MM and its response to treatments have been developed previously. Most of these models have made use of the correlation between MM tumor burden and a protein that is shed by MM cells, M protein, that can be measured in the peripheral blood (Durie and Salmon, 1975; Salmon and Smith, 1970). Sullivan and Salmon (1972) published a simple mathematical model to characterize chemotherapy-induced tumor regression in patients with MM. Swan and Vincent applied optimal control in Swan and Vincent (1977) to predict an optimal chemotherapy dosing strategy for patients with MM. Hokanson et al. (1977) fit individual M-protein data with mathematical models of myeloma cell populations that were sensitive or resistant to chemotherapy. More recently, several groups have examined the disease progression in the presence of various treatments. Jonsson et al. (2015) published a model of patient M-protein levels in response to treatment with carfilzomib. Tang et al. (2016) published a model for patient M-protein levels in clinical trials of bortezomib-based chemotherapy. They predicted that rational combination treatments with decreased selection pressure on myeloma cells could lead to a longer remission period. Nanavati et al. (2017) published a semi-mechanistic protein production and signaling model with seven main compartments. The model was fit to aggregate in vivo xenograft data (digitized from the literature) for mice treated with vorinostat.

These prior studies have not directly examined the role of the immune system in MM disease dynamics, though there is a long history of tumor–immune dynamics models (cf. d'Onofrio, 2005; Kirschner and Panetta, 1998; Kuznetsov et al., 1994; Moore and Li, 2004; de Pillis et al., 2005; Stepanova, 1980; de Vladar and González, 2004). One contribution of our work is the incorporation and careful parameterization of immune-disease interactions in a mathematical model for MM. This is important as several immunomodulatory drugs have been approved for use in patients with MM, and more are currently in clinical trials (Kazandjian and Landgren, 2016). A well-justified model of tumor–immune dynamics would support in silico exploration of regimens that include immunomodulatory therapies.

In Gallaher et al. (2018), we introduced a semi-mechanistic mathematical model of MM (tumor) and immune system dynamics in a hypothetical patient. We focused on the structure of the model, and how best to incorporate tumor–immune dynamics. The mathematical model consists of a dynamical system that tracks tumor and immune components in the peripheral blood of patients with MM. Although MM is a disease based in the bone marrow, myeloma cells overproduce a myeloma protein or M protein, which can circulate outside the bone marrow. Our model uses the level of M protein in the peripheral blood as a surrogate of tumor burden in patients with MM (Durie and Salmon, 1975; Salmon and Smith, 1970). The immune cells included in our model play important roles in disease control or progression, and can also be measured in the peripheral blood. In addition to justifying the structure of the full model, this work also considered a reduced version of the model that still captures key long-term dynamics, and analyzed equilibria and stability of this reduced model.

In this paper, we present methods to determine important components or interactions in the model. This information can be used to help decide which therapies to consider in combination regimens. We began with extensive literature searches to determine and justify parameter values and ranges to use in the model. For the ranges considered feasible for the parameters, we used sampling to perform global sensitivity analyses. We found eight parameters that have the largest effect on long-term levels of M protein. We refer to this subset as "sensitive parameters". We numerically explored how small changes in the sensitive parameters can lead to qualitatively different types of model behavior. In particular, changes in values of the sensitive parameters can result in a *switch* between high and low tumor burden states.

With all except the sensitive parameters fixed, we used identifiability analysis to determine that the model is globally structurally identifiable. In other words, the eight sensitive parameters could be uniquely estimated if we had continuous data from all four populations in our model. Although we did not find time-series data in the literature, we did find steady-state patient values for the four tumor and immune populations included in our model (Greipp et al., 2005; Pessoa de Magalhães et al., 2013; Tang et al., 2016). Fitting to this small amount of data, we were able to explore relationships between the sensitive parameters.

We propose a model for tumor–immune dynamics of multiple myeloma that can be used in future work. The model we propose was developed in Gallaher et al. (2018), has parameter values/ranges we based on literature searches, and has fixed values for all but the eight most sensitive parameters found in this current work. The analysis and findings in this and previous work (Gallaher et al., 2018) add to our overall confidence in the model. If individual-level clinical data become available for each of the four populations in the model, the eight sensitive parameters could be estimated. In silico exploration and optimization could then identify regimens predicted to have best outcomes. Such regimens could be tested either preclinically or clinically and compared to others to evaluate outcomes and calibrate the results.

2. The mathematical model

Our mathematical model, originally presented in Gallaher et al. (2018), consists of a system of ordinary differential equations (ODEs) which represent interactions between myeloma cells and the immune system. We include the following four populations in the peripheral blood, considered as functions of time, t: M protein produced by MM cells, $M(t)$; natural killer (NK) cells, $N(t)$; cytotoxic T lymphocytes (CTLs), $T_C(t)$; and regulatory T cells (Tregs), $T_R(t)$. A detailed description and justification of the model interactions is given in Gallaher et al. (2018). The interactions between the populations are represented in Fig. 1 and summarized in Table 1.

2.1. Model equations

Eqs. (1)–(4) describe the temporal dynamics of M protein, CTLs, NK cells, and Tregs, respectively. The labels **a** - **k** correspond to interactions described in Table 1.

$$\frac{dM}{dt} = s_M + r_M\left(1 - \frac{M}{K_M}\right)M$$
$$- \delta_M\left[1 + \left(\overbrace{\frac{a_{NM}N}{b_{NM}+N}}^{e} + \overbrace{\frac{a_{CM}T_C}{b_{CM}+T_C}}^{f} + \overbrace{a_{CNM}\frac{N}{b_{NM}+N}\cdot\frac{T_C}{b_{CM}+T_C}}^{c}\right)\cdot\right.$$
$$\left.\left(1 - \overbrace{\frac{a_{MM}M}{b_{MM}+M}}^{g,h} - \overbrace{\frac{a_{RM}T_R}{b_{RM}+T_R}}^{j,k}\right)\right]\cdot M$$

$$(1)$$

$$\frac{dT_C}{dt} = r_C\left(1 - \frac{T_C}{K_C}\right)\left(1 + \overbrace{\frac{a_{MC}M}{b_{MC}+M}}^{d} + \overbrace{\frac{a_{NC}N}{b_{NC}+N}}^{b}\right)T_C - \delta_C T_C. \qquad (2)$$

$$\frac{dN}{dt} = s_N + r_N\left(1 - \frac{N}{K_N}\right)\overbrace{\left(1 + \frac{a_{CN}T_C}{b_{CN}+T_C}\right)}^{a}N - \delta_N N \qquad (3)$$
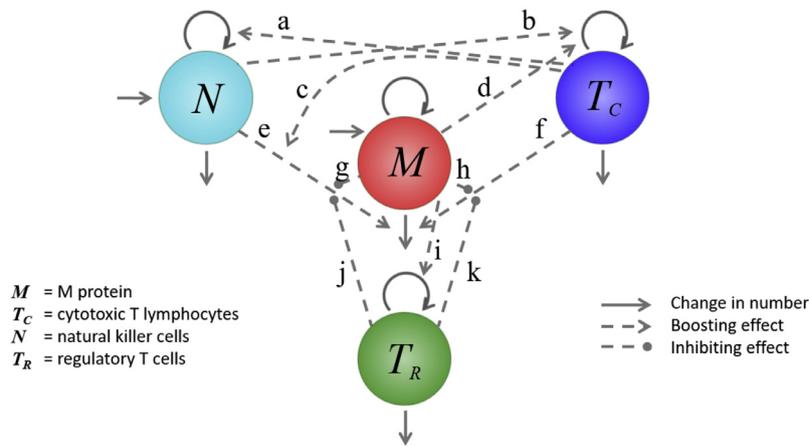
Fig. 1. Diagram of population interactions. M represents M protein produced by MM cells, T_C represents CTLs, N represents NK cells, and T_R represents Tregs. The solid curves represent an increase (arrows pointing in) or decrease (arrows only pointing out) in population sizes. The dashed curves represent interactions that either boost (arrows) or inhibit (solid circles) population sizes or rates of change. These interactions (labeled **a - k**) are summarized in Table 1.

Table 1
Description of interactions between populations in the model.

Label	Interaction	References
a	T_C crosstalk with N; boosts N proliferation	Boyman and Sprent (2012); Lehman et al. (2001); Meropol et al. (1998); Shanker et al. (2010, 2007); Shook and Campana (2011)
b	N crosstalk with T_C; boosts T_C proliferation	Boyman and Sprent (2012); Pallmer and Oxenius (2016); Shanker et al. (2010)
c	T_C increases activation/efficacy of N	Lehman et al. (2001); Meropol et al. (1998); Shanker et al. (2007)
d	Antigens shed from M stimulate T_C proliferation	Abbas et al. (2015); Dhodapkar et al. (2003); Dosani et al. (2015); Janeway (2001); Raitakari et al. (2003); Wen et al. (2002)
e	N cells kill myeloma cells and decrease M	Carbone et al. (2005); Cerwenka et al. (2001); Diefenbach et al. (2001); Frohn et al. (2002); Kawarada et al. (2001); Pratt et al. (2007)
f	T_C cells kill myeloma cells and decrease M	Diefenbach et al. (2001); Kawarada et al. (2001); Wen et al. (2002)
g	Myeloma cells decrease efficacy of N	Gao et al. (2014)
h	Myeloma cells decrease efficacy of T_C	Brown et al. (1998); D'Arena et al. (2016); Feyler et al. (2012); Raja et al. (2012); Suen et al. (2016)
i	Myeloma cells boost T_R proliferation	D'Arena et al. (2016); Favaloro et al. (2014); Feyler et al. (2009, 2012)
j	T_R decreases efficacy of N	Ghiringhelli et al. (2006, 2005); Kim et al. (2007); Smyth et al. (2006); Sungur et al. (2013); Tran (2012)
k	T_R decreases efficacy of T_C	Chen et al. (2005); DiPaolo et al. (2005); Kim et al. (2007); Mempel et al. (2006); Shevach et al. (2006); Tran (2012)

$$\frac{dT_R}{dt} = r_R\left(1 - \frac{T_R}{K_R}\right)\overbrace{\left(1 + \frac{a_{MR}M}{b_{MR} + M}\right)}^{i} T_R - \delta_R T_R \qquad (4)$$

Each population is assumed to grow logistically (with growth rate constants denoted by r_i) and decline exponentially (with loss rate constants defined by δ_i) in the absence of the other populations.

Eq. (1) describes the dynamics of the myeloma cell population, represented by the concentration of M protein in the blood. The population growth includes a constant source term, representing production of similar proteins from sources other than myeloma cells (Dimopoulos et al., 2011). The expanded term multiplying the loss rate constant δ_M describes how this loss rate can be increased or decreased, depending on tumor and immune interactions. In particular, the first part of this term indicates that NK cells (N) and CTLs (T_C) kill myeloma cells (e and f respectively), and that the crosstalk between NK cells and CTLs (c) further increases the efficacy of NK cell killing of myeloma cells. However, myeloma cells (whose levels are assumed proportional to levels of M protein, M) and Tregs (T_R) decrease the efficacy of NK cells and CTLs in their killing of myeloma cells (g, h, j, and k). We use saturating functional forms for feedback (rather than mass action) so that there is a limit to the size of each possible effect.

Eq. (2) describes the dynamics of the CTL population. The proliferation of CTLs is increased by the presence of myeloma and

NK cells (d and b, respectively). Eqs. (3) and (4) describe the dynamics of NK cells and Tregs, respectively. NK cell proliferation is increased by crosstalk with CTLs (a), and Treg proliferation is increased through activation by myeloma cells (i).

2.2. Parameter ranges and values

We performed in-depth literature searches to determine relevant parameter ranges. The details are provided in the Appendix and summarized in Table 2. Given differences in experimental conditions, disease types, as well as variability among patients and uncertainty in the data, we found parameter estimates that differed by orders of magnitudes. We explored possible behaviors of the model for the parameter ranges in Table 2 by performing numerical simulations and sensitivity analyses. All simulations used MATLAB ODE solvers, either ode15s or ode45, with default values used for relative and absolute tolerances unless otherwise indicated.

3. Numerical simulation

We used numerical simulation to explore the spectrum of disease dynamics given by the range of parameter values in our model system.

3.1. Latin hypercube sampling

We created ∼ 10,000 parameter sets (each consisting of 30 parameter values and 4 initial conditions) by sampling the ranges in

Table 2

Table of parameter descriptions and ranges of values used in the model. All parameters are assumed non-negative. M^0, T_C^0, N^0, T_R^0 are used as initial values/conditions. "Number" gives us a way to refer to or order the parameters later. "Base" is used when we need to choose a single value for a parameter. "Bistable" values are used in the section exploring bistability.

Number	Name	Description	Base	Bistable	Range considered	References
-	s_M	Constant source for M	0.001	0.001	0.001 g/(dL·day)	van der Giessen et al. (1975); Gonzalez-Qunitela et al. (2008); Hansen et al. (2014); Mills et al. (2017); Plebani et al. (1989); Stoop et al. (1969)
1	r_M	Growth rate constant for M	0.0175	0.025	0.004–0.5/day	Arciero et al. (2004); Jonsson et al. (2015); de Pillis et al. (2005)
2	K_M	Carrying capacity for M	10	13	7–15 g/dL	Pessoa de Magalhães et al. (2013)
3	δ_M	Natural loss rate constant for M	0.002	0.007	0.001–0.1/day	Hansen et al. (2014); Mills et al. (2017)
4	a_{NM}	Maximum fold-increase in loss rate of M by N	5	5	0–20	Estimated
5	b_{NM}	Threshold for increase in loss rate of M by N	150	275	0–650 cells/µL	Estimated
6	a_{CM}	Maximum fold-increase in loss rate of M by T_C	5	5	0–20	Estimated
7	b_{CM}	Threshold for increase in loss rate of M by T_C	375	500	0–1500 cells/µL	Estimated
8	a_{CNM}	Maximum fold-increase in N efficacy from T_C	8	10	0–20	Estimated
9	a_{MM}	Maximum extent M decreases T_C and N efficacy	0.5	0.35	0–1 ($a_{MM} + a_{RM} \leq 1$)	Estimated
10	b_{MM}	Threshold for M decreasing T_C and N efficacy	3	1.56	0–15 g/dL	Estimated
11	a_{RM}	Maximum extent T_R decreases T_C and N efficacy	0.5	0.64	0–1 ($a_{MM} + a_{RM} \leq 1$)	Estimated
12	b_{RM}	Threshold for T_R decreasing T_C and N efficacy	25	10	0–120 cells/µL	Estimated
13	r_C	Proliferation/activation rate constant for T_C	0.013	0.45	0.01–0.5/day	Arciero et al. (2004); de Boer et al. (1985, 2003); de Pillis et al. (2013)
14	K_C	Carrying capacity for T_C	800	1000	600–1500 cells/µL	Pessoa de Magalhães et al. (2013)
15	δ_C	Loss/inactivation rate constant for T_C	0.02	0.35	0.01–0.5/day	Arciero et al. (2004); de Boer et al. (1985, 2003); de Pillis et al. (2013); Sontag (2017)
16	a_{MC}	Maximum fold-increase in activation rate of T_C by M	5	1	0–10	Estimated
17	b_{MC}	Threshold for increase in activation rate of T_C by M	3	6.5	0–15 g/dL	Estimated
18	a_{NC}	Maximum fold-increase in activation rate of T_C by N	1	1	0–10	Estimated
19	b_{NC}	Threshold for increase in activation rate of T_C by N	150	275	0–650 cells/µL	Estimated
20	s_N	Constant source rate for N	0.03	1.49	0.001–5 cells/(µL·day)	de Pillis et al. (2005); Zhang et al. (2007)
21	r_N	Proliferation rate constant for N	0.04	0.02	0.01–0.5/day	de Pillis et al. (2013, 2005); Zhang et al. (2007)
22	K_N	Carrying capacity for N	450	550	300–650 cells/µL	Pessoa de Magalhães et al. (2013)
23	δ_N	Natural loss/inactivation rate constant for N	0.025	0.025	0.01–0.5/day	de Pillis et al. (2013, 2005); Zhang et al. (2007)
24	a_{CN}	Maximum fold-increase in activation rate of N by T_C	1	1	0–10	Estimated
25	b_{CN}	Threshold for increase in activation rate of N by T_C	375	375	0–1500 cells/µL	Estimated
26	r_R	Proliferation/activation rate constant for T_R	0.0831	0.1	0.01–0.5 cells/(µL·day)	Vukmanovic-Stejic et al. (2006)
27	K_R	Carrying capacity for T_R	80	100	60–120 cells/µL	Pessoa de Magalhães et al. (2013)
28	δ_R	Natural loss/inactivation rate constant for T_R	0.0757	0.077	0.01–0.5/day	Robertson-Tessi et al. (2012); Vukmanovic-Stejic et al. (2006)
29	a_{MR}	Maximum fold-increase in activation rate of T_R by M	2	1	0–10	Estimated
30	b_{MR}	Threshold for increase in activation rate of T_R by M	3	3.25	0–15 g/dL	Estimated
31	M^0	Observed values of M protein in diseased state	4	2.08 or 1.04	0.5–10 g/dL	Greipp et al. (2005); Kyle et al. (2003); Tang et al. (2016)
32	T_C^0	Observed values of CTL in diseased state	464	464	464 ± 416 cells/µL	Pessoa de Magalhães et al. (2013)
33	N^0	Observed values of NK in diseased state	227	227	227 ± 141 cells/µL	Pessoa de Magalhães et al. (2013)
34	T_R^0	Observed values of T_R in diseased state	42	42	42 ± 26 cells/µL	Pessoa de Magalhães et al. (2013)

Table 2. To produce approximately n samples, we first used Latin hypercube sampling (LHS) to generate $2n$ samples in the full rectangular region with $a_{MM}, a_{RM} \in [0, 1]$. In LHS, each parameter range is partitioned into $2n$ equiprobable subintervals. Random samples are then generated with each subinterval sampled exactly once for each parameter. This helps guarantee that the parameter space is evenly covered and the entire range is sampled for each parameter (Iman, 2008). In this paper, each application of LHS assumed uniform distributions of the parameters in the ranges from Table 2. We then restricted to the subspace defined by $a_{MM} + a_{RM} \leq 1$, leaving us with $n = 10,018$ samples. Whenever required, such as in performing local sensitivity analysis or steady-state calculations, the samples were further filtered to remove simulation results leading to numerical instabilities or non-convergence to steady-state solutions. The same 10,018 parameter sets obtained using our LHS sampling procedure were used for preliminary numerical ex-

plorations in this section and sensitivity analysis as described in the next section.

3.2. Range of steady-state values in the population

Using 10,011 parameter sets (7 sets from the original 10,018 generated by LHS were removed due to numerical instabilities), we tested the basic behavior of the model (Eqs. (1)–(4)) by looking at distributions of steady-state values and the distribution of times to reach steady-states. Additionally, we looked for possible distinguishing features, such as immune-cell levels or efficacy values, between the long-term high vs. low M-protein cases.

Simulation results using the specific parameter values listed in the Base column of Table 2 are shown in Fig. 2A. Fig. 2B shows histograms of steady-state values of the model variables using the 10,011 sets of parameter values. The distributions of steady-
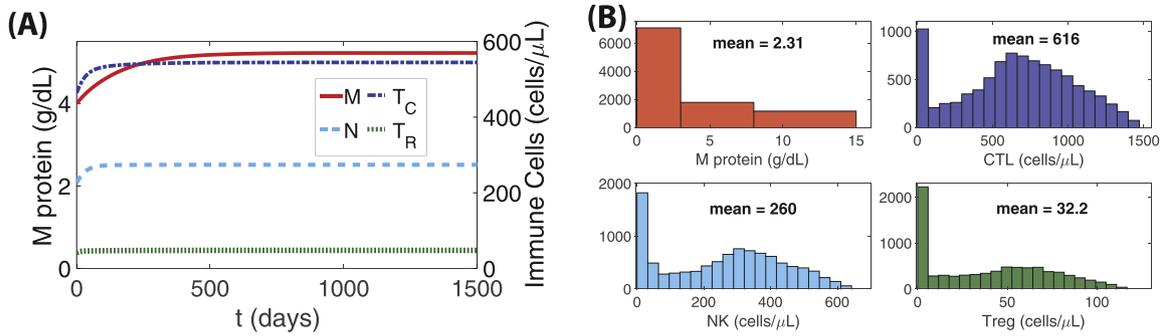
Fig. 2. (A): Dynamics of model variables using parameter values and initial conditions listed in the Base column in Table 2. (B): Histograms of steady-state values of model variables obtained from simulating the model to 6000 days using parameter sets obtained as described in Section 3.1. Out of 10,018 sets of parameter values, 7 sets were removed due to numerical instabilities, leaving a total of $n = 10,011$ sets with population values at time $t = 6000$ days shown here.
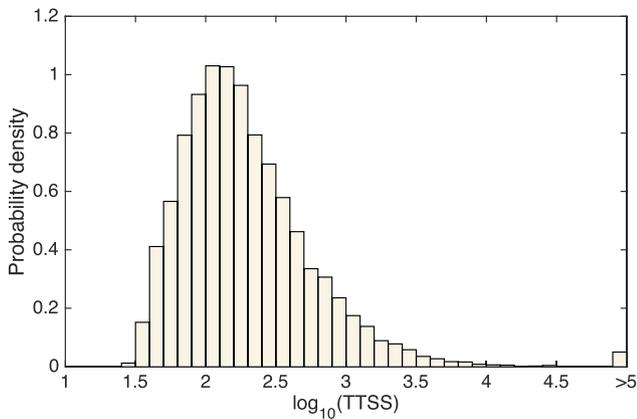

Fig. 3. Histogram of times to steady state (TTSS) for 10,018 simulations normalized so that the total area is one. Time is measured in days and is presented on a log (base 10) scale. Median time is 161 days and mean time is 194 days.

state values are consistent with observations in the literature (Greipp et al., 2005; Pessoa de Magalhães et al., 2013; Tang et al., 2016).

The distribution of times to steady state is analyzed further by plotting the histogram in Fig. 3 (shown in log scale and normalized so that the total area is equal to one). We computed the steady-state solution by simulating the system (1)–(4) until the solution $\vec{y} = (M, T_C, N, T_R)$ satisfied $\frac{\|\vec{y}(t_{i+1}) - \vec{y}(t_i)\|}{\|\vec{y}(t_i)\|} < 10^{-8}$. Out of 10,018 samples, 24.1% reached steady state within 3 months, 54.9% reached steady state within 6 months, and 77.7% reached steady state within one year. On a log scale, the distribution is unimodal with median 161 days and mean 194 days.

3.3. Distinctions between low and high disease burden states

We examined the simulated outcomes further, to see whether certain immune-cell levels or parameter values were associated with high M-protein levels. Specifically, for the simulations with the same 10,018 sets of parameter values, we classified the model outcomes into two categories according to long-term M-protein levels: (1) $M \leq 3$ g/dL ("low"), and (2) $M > 3$ g/dL ("high"). Statistical comparisons between these two cases were made using a two-sided Wilcoxon rank sum test (computed using the `ranksum` command in MATLAB Statistics and Machine Learning Toolbox), a non-parametric test for equality of population medians. The level 3 g/dL is the same M-protein threshold that distinguishes between MM and monoclonal gammopathy of unknown significance (MGUS), which is usually asymptomatic despite elevated M-protein values (Kyle et al., 2011). In addition, data from Pessoa de Magalhães

et al. (2013) suggest that long-term disease control patients with MM have a particular immune signature corresponding to high average CTL counts and slight variations in average NK and Treg cell counts as compared to patients with fully symptomatic MM. We looked for any distinguishing behavior in our model corresponding to either high or low steady-state M-protein values and compared this with the data.

In Fig. 4A, we show box plots of steady-state values obtained by simulations from 10,011 sampled parameter sets. Given the wide range of parameter values considered, there was variability in the results (wide distributions) as reflected by the number of outliers in the box plots. However, our simulation results associated high M-protein levels with lower NK and higher Treg populations than for low M-protein levels. The CTL population did not show the same type of distinction. This is in contrast to data shown in Pessoa de Magalhães et al. (2013) which showed a higher CD8+ immune population for patients with long-term disease control (however, when all effector T cells, CD4+ and CD8+, were combined, the differences between patients with long-term control and those with poor outcome were not as prominent).

We do not expect the steady-state values in our model simulations to reflect the true efficacy of immune cells in keeping the myeloma cell population in check, since we varied all parameter values during sampling, including a_{ij} and b_{ij}. Hence, we computed the size of loss-related terms in Eq. (1) as described in the caption of Fig. 4B. We found that killing terms by both NK and CTL were higher, on average, for the low M-protein case, indicating that both immune populations contribute in killing myeloma cells, in agreement with the results shown in Pessoa de Magalhães et al. (2013). Interestingly, we saw slightly higher CTL steady-state values for the low M-protein case when we performed simulations with fixed feedback killing efficiency parameters (all a_{ij} and b_{ij} were set to the values in the Base column in Table 2 instead of sampled from a range; figure not shown). These results suggest that while CTLs may contribute to lowering M-protein level, the primary mechanisms for controlling myeloma cell levels in the absence of therapy may be due to an increase in NK cell and a decrease in Treg populations.

4. Sensitivity analysis

Due to the high levels of uncertainty and variability in the model parameter values, we performed sensitivity analysis to see if the values of some of the parameters are more important than others in determining the outcome of the system. We used the long-term M-protein level M as the outcome of interest, as M protein continues to be an important measure of tumor burden in patients with MM (Dimopoulos et al., 2011; Durie and Salmon, 1975).
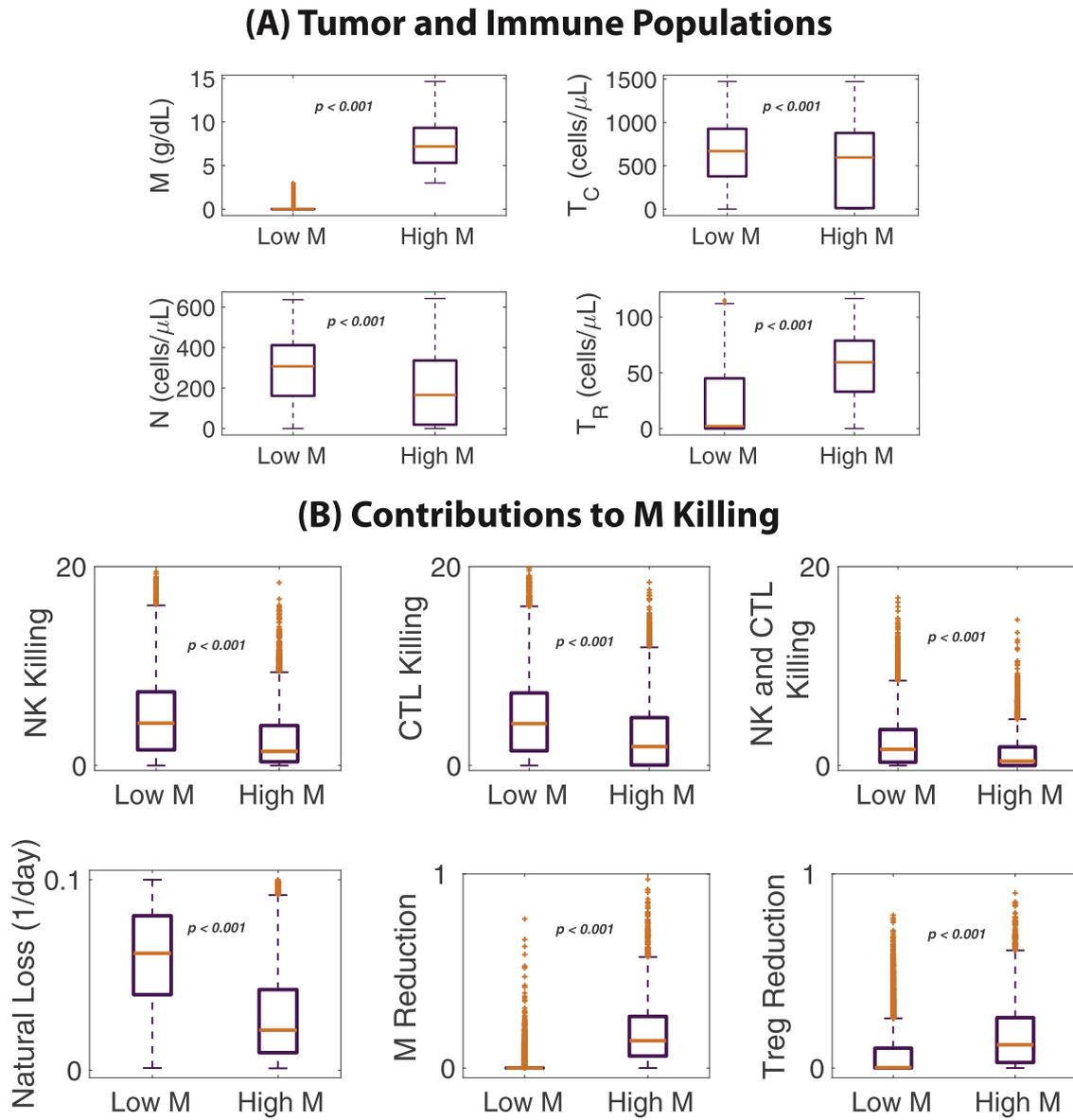
(A) Tumor and Immune Populations

(B) Contributions to M Killing

Fig. 4. Comparison between long-term low M-protein and high M-protein levels. **(A)** Box plots of steady-state values. **(B)** Box plots of sizes of loss terms that appear in Eq. (1): NK Killing, $(a_{NM} N)/(b_{NM} + N)$; CTL Killing, $(a_{CM} T_C)/(b_{CM} + T_C)$; NK+CTL Killing, $(a_{CNM} \cdot T_C \cdot N)/((b_{NM} + N) \cdot (b_{CM} + T_C))$; Natural loss, δ_M; Kill Reduction by M, $(a_{MM} M)/(b_{MM} + M)$; Kill Reduction by Treg, $(a_{RM} T_R)/(b_{RM} + T_R)$. Steady-state values of variables were used to compute killing terms. Model simulation was performed for 6000 days using parameter values sampled from the range listed in the Range Considered column in Table 2. Latin hypercube sampling (LHS) was used to create the 10,018 sets of parameter values as described in Section 3.1; 7 sets were removed due to numerical instabilities (total shown here, $n = 10,011$). For each panel, the result from a two-sided Wilcoxon rank sum test for equality between the two population medians gave $p < 0.001$, indicating that the two population medians are statistically significantly different.

We used two different methods for evaluating parameter sensitivities. Both methods are global, which means that we varied all parameters simultaneously, without fixing any. In the first method, as described in Olufsen and Ottesen (2013), the effects of small parameter changes (local sensitivity) were considered for each parameter set. Global sensitivities for each parameter were then determined by averaging results from local sensitivity calculations. The second method is based on the partial rank correlation coefficients (PRCC), as discussed in Marino et al. (2008), which determines the monotonicity of the relationships between the parameters and the system output.

We explored the parameter ranges listed in Table 2 by considering 10,018 parameter sets, obtained using LHS, assuming uniform distributions on each specified parameter range of values (same sets as used in Fig. 4). We used global methods because we do not assume any of the parameters have values that are a priori well-estimated or do not vary between individuals. Establishing a subset of parameters the system is most sensitive to (a subset we call *sensitive parameters*) allows us to freeze the values of the other parameters without expecting a large impact on the model dynamics. We can then use our best estimate (shown in the Base column in Table 2) for each of these fixed values, and perform identifiability of the system with only the sensitive parameters allowed to vary. If the system is identifiable, then the sensitive parameters can be estimated by fitting the model to appropriate data. The sensitive parameters also represent pathways that may lead to better outcomes when targeted therapeutically, as changes to the sensitive parameters lead to changes in the outcome.

4.1. Sensitivity index and SVD/QR decomposition

The first sensitivity method we used is based on a *sensitivity matrix*. For a given set of parameter values, the sensitivity matrix records the change in the steady-state M value when each parameter is perturbed slightly. As in Olufsen and Ottesen (2013), we constructed a sensitivity matrix with (i, j)th entry corresponding to

$$S_{ij} = \frac{\partial}{\partial p_j}\Big(M(t_i)\Big), \tag{5}$$

where parameter p_j is indexed as in Table 2 ($j = 1, 2, \ldots, 35$) and time t_i is the discrete time point at which M protein is measured ($i = 1, 2, \ldots, K$, for some positive integer K). This gives the sensitivity matrix S, in the following form,

$$S = \frac{\partial M}{\partial p} = \begin{bmatrix} \frac{\partial M}{\partial p_1}(t_1) & \frac{\partial M}{\partial p_2}(t_1) & \ldots & \frac{\partial M}{\partial p_n}(t_1) \\ \frac{\partial M}{\partial p_1}(t_2) & \frac{\partial M}{\partial p_2}(t_2) & \ldots & \frac{\partial M}{\partial p_n}(t_2) \\ \vdots & \vdots & \ddots & \vdots \\ \frac{\partial M}{\partial p_1}(t_K) & \frac{\partial M}{\partial p_2}(t_K) & \ldots & \frac{\partial M}{\partial p_n}(t_K) \end{bmatrix}. \tag{6}$$

Since different parameters can have different units (and thus can have orders of magnitude difference in size), we considered the relative sensitivity $\tilde{S}$ by comparing the size of a relative perturbation in parameter p to the resulting relative change in M (Ingalls, 2013; Olufsen and Ottesen, 2013), i.e.,

$$\tilde{S} = \frac{\partial M}{\partial p}\frac{p}{M}. \tag{7}$$

We approximated the partial derivatives $\frac{\partial M}{\partial p}$ using a finite difference approximation (Olufsen and Ottesen, 2013; Pope et al., 2009), with

$$\frac{\partial M}{\partial p_j}(t_i) \approx \frac{M(t_i; p_j + \epsilon) - M(t_i; p_j)}{\epsilon},$$

where $\epsilon \sim \mathcal{O}(\sqrt{\mathbf{tol}})$ and $\mathbf{tol}$ is the tolerance (size of the absolute error) of the numerical solution of the differential equation. The numerical solutions to the ODE system were obtained by using ode15s in MATLAB with relative and absolute tolerances of $\mathbf{tol} = 10^{-10}$. Thus, the sensitivity matrix has an error of $\mathcal{O}(10^{-5})$ (Olufsen and Ottesen, 2013; Pope et al., 2009).

The sensitivity of each parameter p_j is given by the *sensitivity index*, defined as the magnitude of the corresponding jth column of $\tilde{S}$,

$$\bar{S}_j = ||\tilde{S}_j||_2 = \sqrt{\sum_{i=1}^{K}\left(\frac{\partial M}{\partial p_j}(t_i)\frac{p_j}{M(t_i)}\right)^2}. \tag{8}$$

The values of $\bar{S}_j$ can be ordered from largest to smallest, indicating parameters the model is most sensitive to according to this measure.

For a given parameter set, we computed the relative sensitivity matrix $\tilde{S}$ by simulating the ODE system for 6000 days (with solutions evaluated every 30 days at $t_i = 0, 30, 60, \ldots, 6000$ days). From Fig. 3, approximately 78% of the 10,018 parameter sets described in Section 3.1 had populations that reached steady state within one year. Thus the time period of 6000 days includes both transient dynamics and steady-state values. We examined how parameter values affected steady-state levels of M protein, as well as the transition to steady state. For each parameter set, we recorded the sensitivity index of each parameter (Eq. (8)). For the sensitivity analysis considered here, we discarded 29 of the 10,018 parameter sets, as these resulted in numerical instability or did not reach

Table 3

Ordering of parameters from most to least sensitive with respect to steady-state M-protein level, based on average, or expected, values of the sensitivity index in Eq. (8). Parameter Numbers correspond to the ordering initially listed in Table 2. The expected values $E[\bar{S}_j]$ were obtained by averaging the values $\bar{S}_j$ over 9989 sets of parameter values obtained as described in Section 4.1. For each parameter set, S_j was computed by simulating the system for $5000 \leq t \leq 6000$ days.

Number	Parameter	$E[\bar{S}_j]$	Number	Parameter	$E[\bar{S}_j]$
3	δ_M	28.610	8	a_{CNM}	3.610
1	r_M	25.603	16	a_{MC}	3.133
15	δ_C	20.691	11	a_{RM}	3.038
23	δ_N	19.232	20	s_N	2.392
13	r_C	17.877	17	b_{MC}	2.265
21	r_N	16.268	9	a_{MM}	2.047
4	a_{NM}	11.241	28	δ_R	2.012
22	K_N	10.451	26	r_R	1.860
14	K_C	9.077	12	b_{RM}	1.217
6	a_{CM}	8.426	27	K_R	1.216
5	b_{NM}	7.869	10	b_{MM}	0.931
18	a_{NC}	7.836	29	a_{MR}	0.303
24	a_{CN}	6.272	30	b_{MR}	0.234
7	b_{CM}	5.768	32	T_C^0	0.018
2	K_M	5.518	33	N^0	0.011
19	b_{NC}	5.178	31	M^0	0.006
25	b_{CN}	4.443	34	T_R^0	0.001

steady state within 6000 days (so a total of $n = 9,989$ parameter sets were considered).

In addition to the sensitivity index, we also considered a subset selection approach presented in Olufsen and Ottesen (2013) and Pope et al. (2009) when categorizing parameters as sensitive or insensitive. The rank ρ of the relative sensitivity matrix $\tilde{S}$ is computed by finding the number of singular values of $\tilde{S}$ that are larger than 10^{-4} (since the sensitivity matrix has an error of $\mathcal{O}(10^{-5})$). The rank ρ defines the maximum number of sensitive parameters. The subset of parameters considered sensitive can be found by considering the following matrix decompositions. Given the singular value decomposition (SVD) of the relative sensitivity matrix, $\tilde{S} = U\Sigma V^T$, we partition V into two blocks, $V = [V_\rho\ V_{34-\rho}]$, where V_ρ contains the first ρ columns of V. Then we perform a QR matrix decomposition of V_ρ. That is, we find a permutation matrix P so that $V_\rho^T P = QR$, where Q is an orthogonal matrix and R is an upper triangular matrix whose diagonal elements are arranged in order of decreasing magnitude (Golub and Van Loan, 2012). The permutation matrix P can then be used to determine the ordering of parameter sensitivity, $\hat{\theta} = P^T\theta$, where $\theta = [1, 2, \ldots, 34]^T$ and the first ρ entries of $\hat{\theta}$ determines the group of parameters that may be considered sensitive.

4.1.1. Sensitivity of steady-state M values

To examine the sensitivity of the steady-state value of M to changes in each parameter, we recorded the sensitivity index from Eq. (8) for each parameter evaluated for t_i between 5000 and 6000 days. Results from 9989 different parameter sets (those that reach steady states within 6000 days) are shown in Table 3. The average, or expected, value of the sensitivity index in Eq. (8), $E[\bar{S}_j]$, is listed for each parameter p_j. The distribution of sensitivity index $\bar{S}_j$ values over the 9989 parameter sets is shown by parameter in the box plot in Fig. 5.

4.1.2. Sensitivity of transient M dynamics

We also examined how parameter values may change the time course of M from initial to steady-state conditions by analyzing the relative sensitivity matrix $\tilde{S}$ for the system evaluated from 0 to 6000 days. The sensitivity index ordering of parameters listed in Table 3 was preserved. However, subset selection using SVD/QR decompositions gave slightly different results. In Fig. 6A, we show
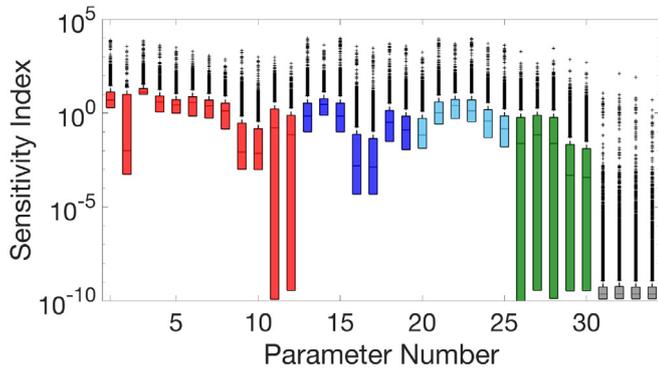
Fig. 5. Box plot of steady-state sensitivity index value $\bar{S}_j$ for each parameter number $j = 1, 2, \ldots, 34$ (in the order listed in Table 2) for the same 9989 parameter sets used for Table 2. The boxes of sensitivity index values for parameters directly affecting the M population are colored in red, the CTL population in dark blue, the NK cell population in light blue, and the Treg population in green. Sensitivity indices for the initial conditions are colored in gray. (For interpretation of the references to color in this figure legend, the reader is referred to the web version of this article.)

the fraction of times (among 9989 parameter sets) that a particular parameter is characterized as sensitive. The initial value of M, M_0, was characterized as sensitive for all parameter sets, as it significantly impacts values of M at early times. Parameters governing the dynamics of M in the absence of immune cells, namely δ_M, K_M, and r_M, were characterized as next-most sensitive. Fig. 6B shows the distribution of singular values. Fig. 6C shows the fraction of times that the relative sensitivity matrix $\tilde{S}$ has a particular rank. A rank between five and eight appears most often, with each appearing in more than 10% of trials (a total of 55% of 9989 parameter sets considered have rank between five and eight). We used this result to conclude that likely at most eight parameters can be considered sensitive.

4.2. Partial rank correlation coefficients

The second sensitivity method we used was the method of partial rank correlation coefficients (PRCC), as discussed in Marino et al. (2008). PRCC can be used when the relationships between the model parameters and the model output are nonlinear, as long as the relationships are monotonic (Kendall, 1942). To com-

pute the PRCC, the data are first rank-transformed. That is, for each parameter/output, we take the 10,018 values generated by LHS, and map them to the set $\{1, 2, \ldots, 10018\}$ according to their rank from lowest to highest, keeping track of which sample parameter set they came from. This transforms all monotone relationships into linear ones, and thus removes any correlation issues due to non-linearity so long as the relationships are still monotone. The partial correlation coefficient between a rank-transformed parameter p_j and system output y is then computed as the correlation coefficient between the two residuals $(p_j - \hat{p}_j)$ and $(y - \hat{y})$, where $\hat{p}_j$ and $\hat{y}$ are linear regression models in terms of the remaining parameters (Marino et al., 2008). A PRCC value of 1 indicates a strictly increasing relationship, while a PRCC value of -1 indicates a strictly decreasing relationship. In this work, PRCC was computed using the `partialcorr` function in MATLAB 2014b using 10,018 LHS samples.

Sensitivity coefficients and the corresponding p-values for each parameter are listed in Table 4 and displayed graphically in Fig. 7A. The sensitivity analysis shows that there are 27 parameters that have a statistically significant PRCC value, assuming a p-value cutoff of 0.01. There are 7 parameters that have statistically insignificant PRCC values, including all four initial conditions. The PRCC results indicate that the system is most sensitive to the loss and growth rate constants of M (δ_M and r_M, respectively). The results also indicate that the system is highly sensitive to the growth and loss rate constants of T_C and N (r_C, δ_C, r_N, and δ_N) and the effects of N and T_C on M, and that the system is less sensitive to parameters directly related to T_R and to the four initial conditions.

4.3. Comparison of sensitivity index and PRCC methods

We compared the parameter sensitivity results in Tables 3 and 4, obtained using two different global sensitivity methods. Of the ten most sensitive parameters determined by each method (the first ten listed in each Table), there are eight parameters shared in common. These are δ_M, r_M, δ_N, r_N, δ_C, r_C, a_{NM}, and a_{CM}. This subset of eight parameters includes growth and loss rate constants for M, T_C, and N, and the efficacy rate constants for T_C and N. We note that parameters directly related to T_R do not appear in this subset. This appears to be in agreement with the data in Pessoa de Magalhães et al. (2013) that show there are not significant differences in Treg levels between healthy adults and patients with various stages
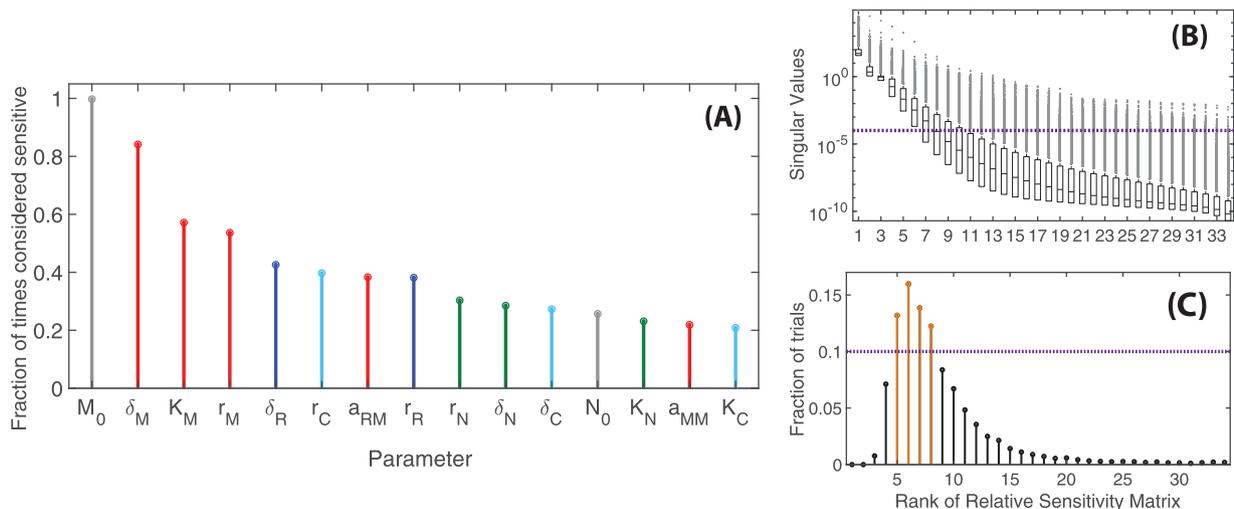

Fig. 6. Results from the subset selection approach using SVD/QR decomposition. **(A)** Fraction of trials for which the given parameter was characterized as sensitive over the full time course by the SVD/QR subset selection method. Only parameters that were characterized as sensitive at least 10% of times (from 9989 parameter sets) are shown. **(B)** Box plot of singular values of $\tilde{S}$ (dashed line shows the threshold value of 10^{-4} for computing the matrix rank). **(C)** Histogram of values of Rank($\tilde{S}$) (dashed line shows the threshold for 10% of all trials).

Table 4

Table of PRCC values by parameter, in order of descending magnitude, and their corresponding p-values (p-values smaller than 10^{-14} are rounded to 0). The response variable is the steady-state value of M. Results were obtained using LHS with 10,018 samples (samples as described in Section 3.1). For each sample, steady state is determined as in Section 3.2.

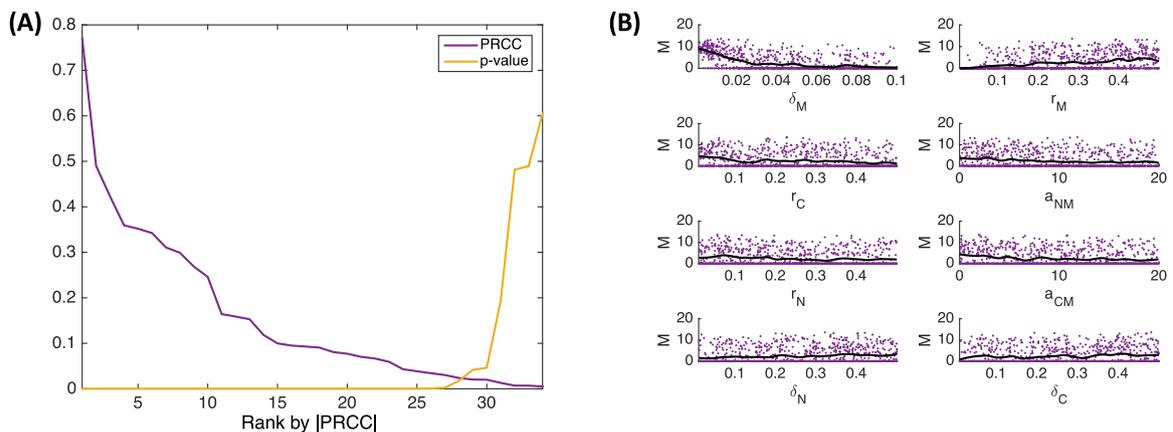| Parameter	PRCC	p-value	Parameter	PRCC	p-value
δ_M	−0.77038	0	K_N	−0.090636	0
r_M	0.48974	0	b_{NC}	0.080751	0
r_C	−0.42271	0	r_R	0.07711	1.2031e−14
a_{NM}	−0.35933	0	b_{CN}	0.070195	2.187e−12
r_N	−0.3518	0	b_{RM}	−0.066549	2.8053e−11
a_{CM}	−0.34242	0	s_N	−0.059274	3.0767e−09
δ_N	0.31079	0	a_{MC}	−0.043035	1.6946e−05
δ_C	0.2991	0	b_{MM}	−0.038472	1.2041e−04
b_{NM}	0.26877	0	b_{MC}	0.034305	6.0694e−04
b_{CM}	0.24588	0	a_{MR}	0.030291	0.0024691
a_{CN}	−0.16422	0	T_R^0	−0.02378	0.01749
a_{NC}	−0.15877	0	a_{MM}	0.020392	0.041591
a_{CNM}	−0.15286	0	K_R	0.019943	0.046287
K_M	0.11825	0	N^0	−0.013022	0.19323
δ_R	−0.099828	0	M^0	−0.0070448	0.48151
a_{RM}	0.095047	0	b_{MR}	0.0069206	0.48928
K_C	−0.092935	0	T_C^0	−0.0051749	0.60513

Fig. 7. (A): Plot of the absolute value of PRCCs and p-values for 34 parameters (s_M fixed), ranked from highest to lowest magnitude of PRCC. **(B):** Scatter plots of steady-state M values vs. the eight most-sensitive parameters, with 1000 samples shown. Black curves indicate a loess (local regression) fit to the data.

of MM. Scatter plots of the steady-state M values vs. the eight sensitive parameters are shown in Fig. 7B.

We conclude this section by noting that the parameter sensitivity approaches we took allow us to select a subset of parameters that appear to be the most sensitive for model outcomes. This has two important consequences. One is that it can help identify potentially important pathways that can alter the progression of disease. The second is that it can indicate a parameter subset that can be fit to available data. In the next section, we focus on this second aspect. We fix the least-sensitive parameters to values we identified in the literature (listed in the Base column of Table 2) and only vary the eight most-sensitive parameters, namely: r_M, δ_M, r_C, δ_C, r_N, δ_N, a_{NM}, and a_{CM}.

4.4. Small changes in MM growth and loss rates can switch disease state - a consequence of model bistability

We next show numerical simulations that illustrate how slight changes in the values of the most sensitive parameters can shift the model outcome between high and low M-protein steady state values, representing states of high tumor burden and long-term disease control (LTDC), respectively. These results indicate that our model exhibits bistability, a result that was also identified for a reduced version of our model in which NK cells and Tregs were held fixed (Gallaher et al., 2018). It is important to note that we

can not determine bistability a priori from the eigenvalues of the associated Jacobian matrix. This is because we can not analytically compute all model steady states (required for the Jacobian analysis), since they are the zeros of a high-degree polynomial.

Before we show how small changes in the values of the sensitive parameters can lead to different model outcomes, we simulate using a parameter set that demonstrates bistability. In particular, we show how different initial M-protein levels can lead to different model outcomes.

Fig. 8A corresponds to high tumor burden (achieved for a larger M initial condition), while Fig. 8B represents a state of disease control (achieved for a smaller M initial condition). For each simulation, we initialize our model using immune cell counts that correspond to a diseased state (Pessoa de Magalhães et al., 2013), where we assume a diseased individual to have an M-protein level higher than 1.5 g/dL (Stoop et al., 1969). The scale to the right of each figure corresponds to immune cell concentrations (T_C, N and T_R), while the scale to the left of each figure corresponds to M-protein concentration (the solid red curves represent the M-protein concentration over time). The steady-state value for M in the case of higher tumor burden is 3.37 g/dL, and is 0.16 g/dL for disease control.

In Fig. 8A, we initialized M protein to a value of 2.08 g/dL. In this case, we note an immune response, where both NK cell
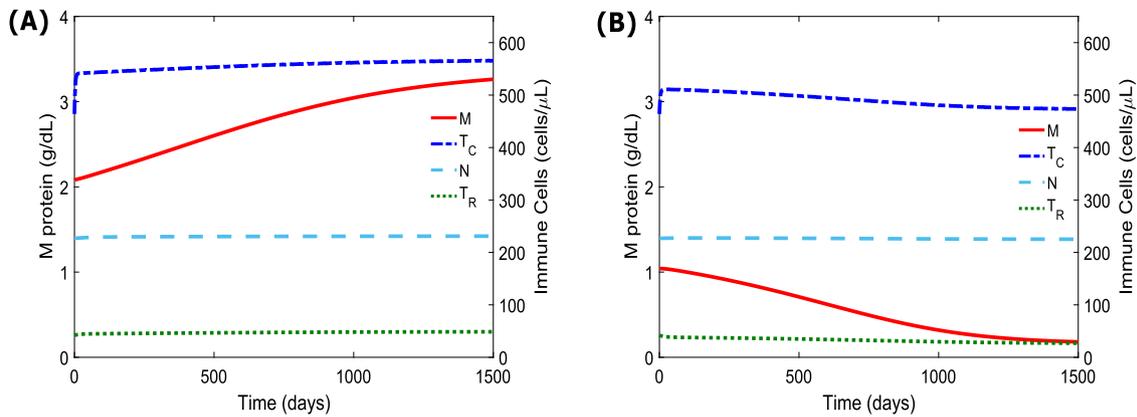
Fig. 8. Simulations with the initial condition for M varied. Initial conditions, corresponding to a diseased state (Pessoa de Magalhães et al., 2013), are set as $T_C(0) = 464$, $N(0) = 227$, and $T_R(0) = 42$. The scale on the right corresponds to immune cells T_C, N, and T_R, and the scale on the left corresponds to M-protein concentration (solid curve). **(A)** $M(0) = 2.08$. The final M-protein level is 3.37. **(B)** $M(0) = 1.04$. The final M-protein level is 0.16. For both simulations, other parameter values are those shown in the Bistable column in Table 2. $s_M = 0.001$, $r_M = 0.025$, $\delta_M = 0.007$, $r_C = 0.45$, $\delta_C = 0.35$, $s_N = 1.49$, $r_N = 0.02$, $\delta_N = 0.025$, $r_R = 0.1$, $\delta_R = 0.077$, $b_{NM} = 0.5 * K_N$, $b_{CM} = 0.5 * K_C$, $b_{MM} = 0.12 * K_M$, $b_{RM} = 0.1 * K_R$, $b_{MC} = 0.5 * K_M$, $b_{NC} = 0.5 * K_N$, $b_{CN} = 0.375 * K_C$, $b_{MR} = 0.25 * K_M$, $a_{NM} = 5$, $a_{CM} = 5$, $a_{CNM} = 10$, $a_{MM} = 0.35$, $a_{RM} = 0.64$, $a_{MC} = 1$, $a_{NC} = 1$, $a_{CN} = 1$, $a_{MR} = 1$. The carrying capacities are: $K_M = 13$, $K_C = 1000$, $K_N = 550$, and $K_R = 100$.

and CTL populations increase (although NK cells increase only marginally). However, this immune response is not enough to lower the tumor burden. Here, the steady-state value for M-protein is high (3.37 g/dL), and the steady-state values for the immune cell populations are 567, 231, and 49.0 cells/μL for CTLs, NK cells, and Tregs, respectively.

In Fig. 8B, we initialized an M-protein level of 1.04 g/dL. The CTL population increases slightly at first, the NK cell population remains near constant, and the Treg population decreases. As the M-protein levels progressively decrease to a state of disease control (steady-state value of M-protein 0.16 g/dL), the immune response is suppressed (the CTL population drops). The steady-state values for the immune cell populations are 472, 225, and 26.5 cells/µL for CTLs, NK cells, and Tregs, respectively.

We illustrate the model sensitivity by numerically showing the effect of varying sensitive δ_M and r_M on final M steady-state values. By doing so, we create a similar *switch* in the model outcome (similar to the above bistable result). In Fig. 9, we use the same initial conditions as in our bistable result in Fig. 8. The figures on the left correspond to high initial values of M ($M(0) = 2.08$), and those to the right correspond to low initial values of M ($M(0) = 1.04$). The solid and dashed curves show the M-protein levels, demonstrating the different possible outcomes due to a small variation in the indicated parameter.

One of the goals of this work is to refine our original model so that it can be used in the future to explore optimal treatment regimens. The results shown here emphasize the need for not only a careful exploration of model sensitivity, but also a careful exploration of model behavior, and in particular model bistability.

5. Identifiability

Model identifiability is an important step that considers the possibility of obtaining unique parameter values from data. *Structural identifiability* considers the problem of fitting parameters to perfect data, continuous in time and space, and is related to model structure and independent of the parameter values. *Practical identifiability* considers the problem for more realistic data availability and error within. We consider both types in this section.

There are three possible outcomes for model structural identifiability: 1) globally identifiable, corresponding to a case in which parameters can be estimated uniquely to error-free data, 2) locally identifiable, corresponding to a finite number of parameter values that can equally well fit the data, and 3) non-identifiable, corre-

sponding to a case in which there is not enough information to obtain parameters from error-free data. The nonlinear nature of our model (common for tumor–immune models) is typically a challenge in obtaining parameter identifiability. Indeed we were not able to establish identifiability of our full model, which indicates it may not be possible to obtain all parameter values uniquely or non-uniquely from error-free data for the four model populations.

In this section, we consider whether the subset of eight sensitive parameters determined in Section 4, can be uniquely estimated from measurements of values of M, T_C, N, and T_R. This is similar to the approach in Balsa-Canto et al. (2010). We examine both structural identifiability (assuming error-free measurements at all times) and practical identifiability (data with measurement error, only available at discrete times). Structural identifiability should be checked before the model is fit to data. If a model is structurally non-identifiable, then any parameter estimates obtained numerically should not be relied on.

5.1. Structural identifiability

There are multiple approaches for computing structural identifiability. We analyzed our model using the MATLAB package GenSSI (Chiş et al., 2011), which handles nonlinear systems of differential equations by applying a power series approach. Briefly, GenSSI uses Lie derivatives of the model system in order to construct a system of equations; the solvability properties of these equations provide information about the global and local structural identifiability as well as non-identifiability.

One feature of GenSSI is that in addition to providing expressions for the solutions to algebraic relations, it also provides a graphical representation through the generation of *identifiability tableaus* (Chiş et al., 2011). Identifiability tableaus, as shown in Fig. 10, are binary representations of the Jacobian of the series coefficients with respect to the parameters. Each column represents a parameter, and each row shows which of the series coefficients are non-zero (shown as black in the tableau) (Balsa-Canto et al., 2010). The structure of the tableau is used to help decide how to solve equations for a particular parameter (Balsa-Canto et al., 2010; Chiş et al., 2011). Specifically, the GenSSI Jacobian matrix rank obtained by taking a predefined set of derivatives must match the number of unknown model parameters in order for local identifiability to be guaranteed.

For the generated model tableaus, if a parameter column consists solely of zeros, then that parameter cannot be identified. If a
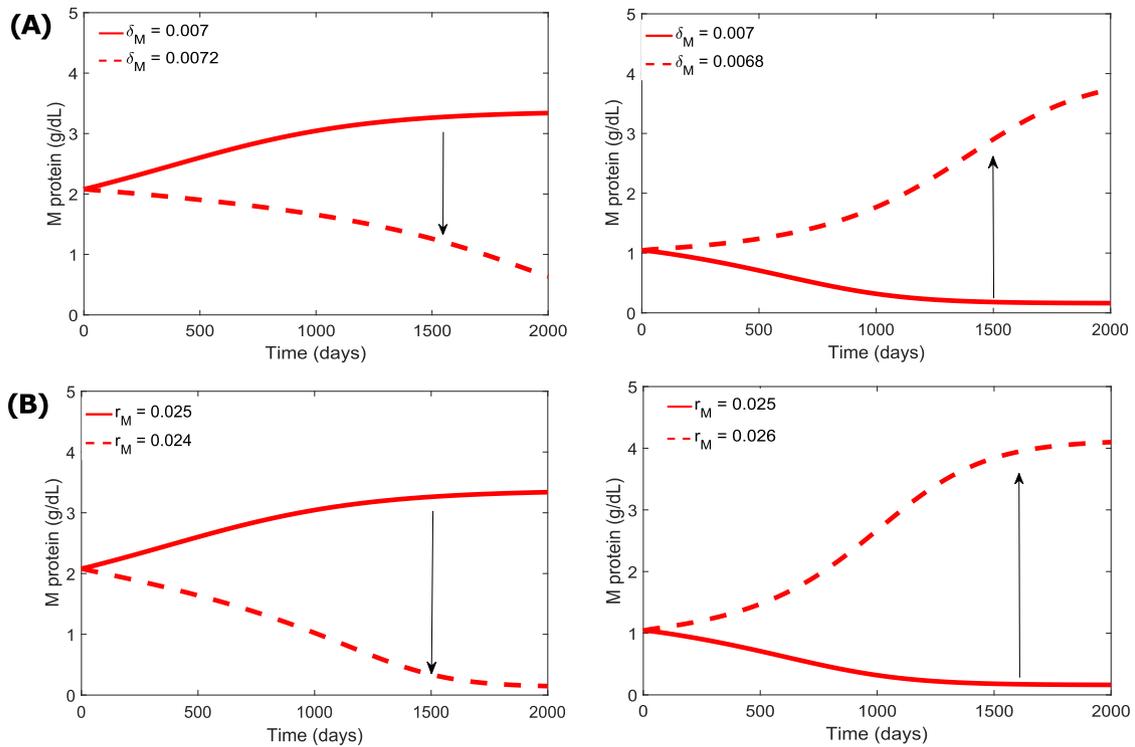
Fig. 9. Effect of small changes in δ_M and r_M values on M. The plots on the left have higher initial M values ($M(0) = 2.08$) than the plots on the right ($M(0) = 1.04$). The solid and dashed curves show different M-protein dynamics for slight differences in values of the indicated parameters. **(A):** Effect of varying δ_M. We show a switch from state of high tumor burden to long-term disease control (LTDC) for increasing δ_M (left), and a switch from a state of LTDC to a state of high tumor burden for decreasing δ_M (right). **(B):** Effect of varying r_M on final M values. We show a switch from state of high tumor burden to LTDC for decreasing r_M (left) and a switch from state of LTDC to a state of high tumor burden for increasing r_M (right). All parameters used here are listed in Table 2 in the Bistable column.
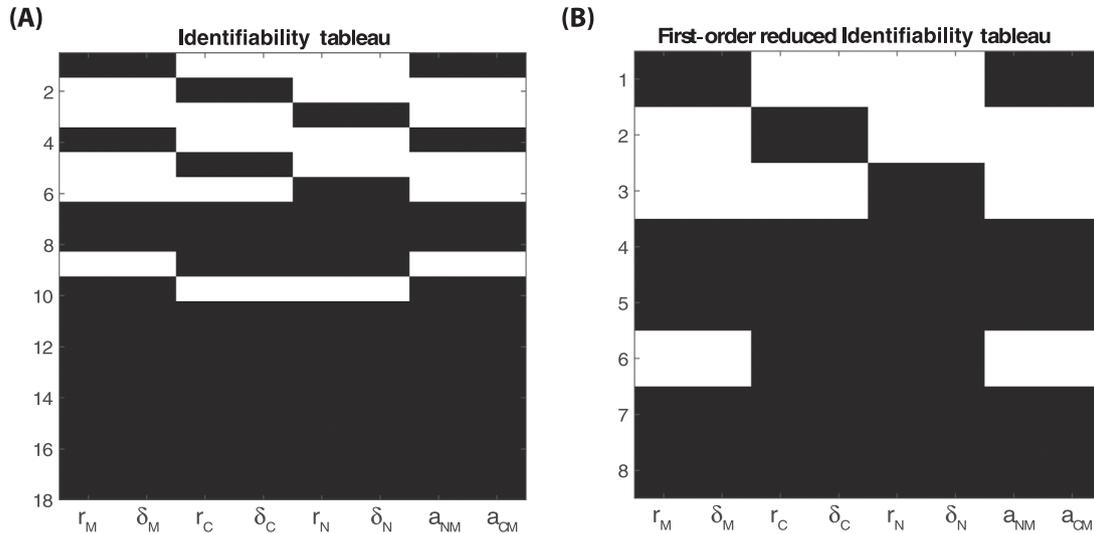

Fig. 10. Model identifiability results with the subset of eight parameters the model is most sensitive to. **(A):** Identifiability tableau. **(B):** Results and reduced tableau. All eight parameters shown are globally identifiable. The structurally globally identifiable parameters are: r_M, δ_M, r_C, δ_C, r_N, δ_N, a_{NM}, and a_{CM}. For the generated tableaus, values of one are represented as black, and values of zero are represented as white. Columns consisting solely of zeros indicate that the respective parameter cannot be identified and rows consisting solely of zeros provide no information and are deleted. A row consisting of a single non-zero (black) entry indicates that the corresponding parameter is structurally identifiable. Tableau rows that consist of two or more ones indicate that there are relations that must be solved algebraically as detailed in Chiş et al. (2011). When parameters from the identifiability tableau in (A) can be computed as functions of the power series coefficients and eliminated, then a *reduced* tableau shown in (B) is obtained.

row consists of a single one (shown as a black rectangle) then the parameter is structurally identifiable, whereas multiple ones in one row indicates that there are relations that might be solved to provide identifiability (Chiş et al., 2011). We obtain an identifiability tableau in Fig. 10A (note that sometimes this is referred to as minimum tableau of rank equal to the number of parameters, i.e., rank eight in our case) that shows 18 non-zero rows/generating series

coefficients that depend on the model parameters (dependency marked in black on the tableau). If any parameters from the identifiability tableau can be computed as functions of the power series coefficients and eliminated, then a *reduced tableau* is obtained, as shown in Fig. 10B. Using the reduced tableaus the GenSSI algorithm solves for the parameters and in our case we obtain unique solutions for the algebraic relations that arise for the parameters.

So with the subset of eight most-sensitive parameters allowed to vary, the model is globally structurally identifiable, which indicates that error-free time series data for the four relevant model populations would be sufficient to identify a unique subset of eight parameters.

When we added one or more parameters to the list of eight free parameters (for example, by adding one or more carrying capacity parameters, which rank high in sensitivity), we obtained only locally identifiable results. We say that the eight most-sensitive parameters are a priori identifiable. Next, we pursue practical (or a posteriori) identifiability. That is, we test whether it is possible to evaluate parameters from a specified set of experimental data subject to experimental noise, explored in the next section.

5.2. Practical identifiability

Given the structural identifiability for the model with the eight sensitive parameters allowed to vary, we subsequently examined its practical identifiability. Structural identifiability assumes the availability of noiseless, complete time-series data. In practice, such data are not available; thus we also explored whether the eight most-sensitive parameters are identifiable from noisy steady-state data. In this section, we seek to determine whether a distribution with a clear mode can be determined for each of the eight sensitive parameters given such data.

To estimate the parameter distributions, we used a Markov Chain Monte Carlo (MCMC) method with Metropolis-Hastings sampling, which we ran in MATLAB as in Hastings (1970). Given data for the system output, MCMC is a method for sampling the posterior distributions of parameter values given a prior distribution and a likelihood function that is known (up to constant scaling). It achieves this by constructing a Markov chain whose stationary distribution is the posterior distribution of interest (Brooks, 1998). At each iteration of the Markov chain, a new parameter set is proposed; the proposed parameter set is then accepted or rejected according to an acceptance criterion. We used the Metropolis-Hastings updating scheme which, given a symmetric proposal distribution and uniform prior distribution, accepts the new sample with probability given by the ratio of the new likelihood to the old likelihood (Hastings, 1970). In this work, prior distributions for the parameters were taken to be uniform within the ranges in Table 2, with the growth and loss rate constants (r_i and δ_i, respectively) taken on a log (base 10) scale for each $i \in \{M, T_C, N\}$.

If we assume that patients are at a steady state at the time of diagnosis, we can use certain clinical data to try to infer parameter values. Pessoa de Magalhães et al. (2013) provide means and standard deviations for the three immune cell populations (T_C, N, T_R) for patients with MM. These are listed in Table 2 as "mean ± standard deviation" in the Range Considered column. We used a mean of 3.9 g/dL for M in patients prior to treatment (cf. Greipp et al., 2005; Tang et al., 2016). The standard deviation data for M protein was estimated as 1 g/dL based on data shown in Tang et al. (2016). We additionally assumed that the cell populations are log-normally distributed and bounded by the ranges in Table 2.

We used a chain length of 100,000 with a burn-in period of 10,000 iterations. The resulting parameter distributions are presented in Fig. 11 in the form of one-dimensional histograms and two-dimensional heat maps. Many of the parameters have broad distributions and thus are not practically identifiable given the available steady-state data. This is not surprising given the limited amount of data (steady-state values for the four populations) and the large amount of uncertainty in the data (as evidenced by the large standard deviations). In particular, the standard deviation of the T_C population size is almost as large as the mean. However, it is clear from Fig. 11 that $\log(r_M)$ and $\log(\delta_M)$ have a strong linear relationship. Thus, while the parameters themselves are not iden-
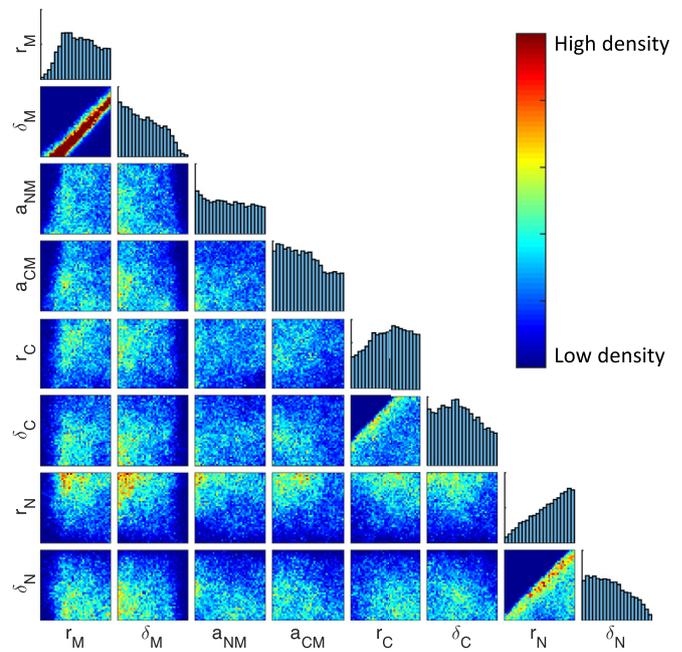

Fig. 11. Matrix of two-dimensional heat maps showing the parameter distributions obtained using MCMC, with one-dimensional histograms on the diagonal. In the heat maps, red indicates areas of high density and blue indicates areas of low density, as shown in the temperature guide in the upper right. The axis limits are given by the parameter ranges in Table 2. Axes for r and δ parameters are on a log (base 10) scale. (For interpretation of the references to color in this figure legend, the reader is referred to the web version of this article.)
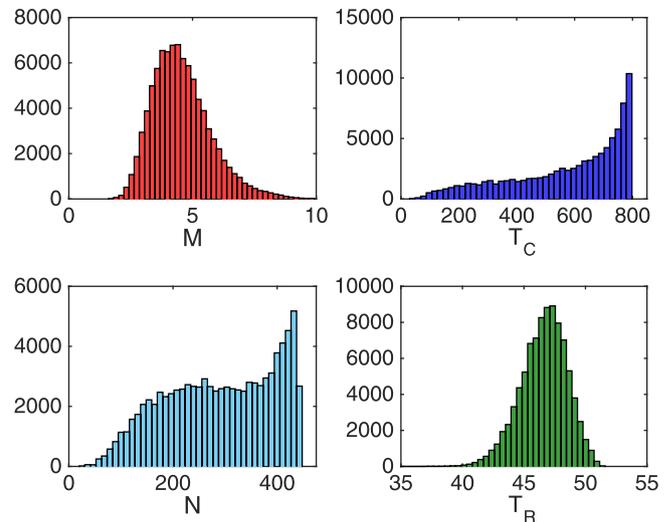

Fig. 12. Distributions of the four populations M, T_C, N, and T_R for the MCMC chain.

tifiable, a combination of them is identifiable. Similarly, the heat maps reveal linear inequalities between $\log(r_C)$ and $\log(\delta_C)$ and between $\log(r_N)$ and $\log(\delta_N)$.

Fig. 12 shows the distributions for the four populations M, T_C, N, and T_R for the MCMC chain. While the M distribution matches the assumed distribution well, the immune cell populations do not match the data well. In particular, the T_C and N compartments tend toward their respective carrying capacities and cluster there, while the T_R compartment size is tightly controlled. This may indicate that by fixing some of the parameters deemed less sensitive, we are neglecting their influence in controlling these cell populations. For example, since the growth/loss rate constants and carrying capacity of T_R are fixed, we would expect its steady-state population

size to have small variance. This is in agreement with the data in Pessoa de Magalhães et al. (2013), in which the Treg populations are similar between healthy volunteers and patients with various stages of MM.

6. Conclusion

In this work, we explored a mathematical model of tumor–immune dynamics for MM that we originally presented in Gallaher et al. (2018). Our model uses M-protein and immune cell populations in the peripheral blood to represent the dynamics of disease burden and immune response in a patient with MM. The value of a model depends not only on the model structure, but also on the parameter values used with the model. In Gallaher et al. (2018), our focus was on the model structure; in this new work, our focus was to carefully determine and justify parameter values and ranges, evaluate parameter sensitivity and model identifiability, and to explore relevant model behavior. Although our objective was to analyze a specific mathematical model, the techniques we present are applicable to mathematical models more broadly.

We applied two different global sensitivity methods, and found that the top ten sensitive parameters for each method (results shown in Tables 3 and 4) have eight parameters in common. These are δ_M, r_M, δ_C, δ_N, r_C, r_N, a_{NM}, and a_{CM}. The SVD/QR decomposition results support up to eight sensitive parameters, so we propose that this set of eight parameters is the maximum set of sensitive parameters to be considered for this model.

We allowed these eight most sensitive parameters to vary in explorations of the model, while we kept the values of the other parameters fixed. Small changes in the sensitive parameters can produce large changes in the steady-state value of M. The sensitive parameters thus may indicate vulnerabilities in the model pathways, which can guide the choice of therapeutic interventions to try in combination.

The behavior of the model for different values of two highly-sensitive parameters, δ_M and r_M, is shown in Fig. 9. This change in behavior (switching between high tumor burden and disease control) is a consequence of the fact that there are certain parameter sets for which our model exhibits bistable behavior. Numerical simulation (not shown) suggests the set of parameter values for which bistability occurs may be small, which indicates that further investigation of model behavior may be needed in future work.

Limitations of our model include the following: (1) our model tracks populations in the peripheral blood, although many of the interactions that drive our model dynamics occur in the bone marrow and lymph nodes; (2) we use M protein in the peripheral blood as a measure of tumor burden, which correlates with tumor burden (Durie and Salmon, 1975; Salmon and Smith, 1970) but is an indirect measurement of tumor burden; (3) we have limited our model to a small number of immune cell types, although others may also be important (Dosani et al., 2015; Kawano et al., 2015); and (4) our model includes terms in Eq. (1) that represent immune system removal of M protein even in the absence of disease, which may not be accurate. Additionally, our ability to estimate parameters for this model would be improved if time series data were available from individual patients with MM who have not yet been treated, perhaps from historical data sets.

The careful parameter estimation, the work to determine sensitive parameters in the model, the identifiability analysis, the re-examination of parameter values for the sensitive parameters, and the numerical simulations, all add confidence to the structure and the parameter values of the model. This model could be used in other work similarly focused on steady-state M-protein values, with the eight most-sensitive parameters allowed to vary, and the others fixed to values in the Base column of Table 2. The

work done here provides the necessary foundation for natural next steps: the prediction of optimal combination regimens for patients with MM, and the experimental validation of such a prediction.

Appendix A. Determination of parameter ranges and values

We provide the details of literature information related to parameters in our model, and explain our calculations and decisions for the parameter values and ranges summarized in Table 2.

Growth and loss parameters for M protein, M

Normal plasma cells produce immunoglobulin (Ig), which has multiple types. A patient with MM typically overproduces one immunoglobulin type, with the majority of patients overproducing IgG and most other patients overproducing IgA (Kyle et al., 2003). We used values associated with IgG whenever a choice had to be made for patients with MM (Greipp et al., 2005; Tang et al., 2016).

Constant source term, s_M: In healthy adults, a typical level of IgG in the peripheral blood is approximately 1 g/dL (van der Giessen et al., 1975; Gonzalez-Qunitela et al., 2008; Plebani et al., 1989; Stoop et al., 1969). In the absence of myeloma ($r_M = 0$ in healthy cases), we reduced Eq. (1) to $dM/dt = s_M - \delta_M M$. Using $\delta_M = 0.001$/day (the low end of the range determined in the δ_M section below) and a steady-state value of $M_{ss} = 1$ g/dL yields $s_M = 0.001$ g/(dL·day). The s_M term is the only term in our model that is not related to MM. Additionally, global sensitivity analysis (not shown) indicates that the model is only sensitive to s_M when levels of M are around 1 g/dL or lower. Thus we fixed s_M to a value of 0.001 g/(dL·day), as we focused on patients with MM.

Growth rate constant, r_M: The mathematical model of Jonsson et al. (2015) for M-protein levels in patients with MM lists an M-protein growth rate constant of 0.0283/week ≈ 0.004/day, which corresponds to a doubling time of $\ln(2)/0.004 \approx 173$ days.

In Nardiello et al. (2011), a plasma cell proliferation index (PCPI) assay was used to determine the fraction of cells undergoing proliferation in MM cell samples from the bone marrow of patients. Due to the design of the PCPI assay, which measures the proliferation marker Ki-67 in cells, the resulting values are over-estimates. The lowest value in that work was 6.9%, which was for the group of newly-diagnosed patients. Kumar et al. (2004) used bromodeoxyuridine (BrdU) to assess proliferation of myeloma cells from patients (as a percentage of cells entering S phase during the incubation time). The labeled cells had median values of 0.4% and 1.2% in samples from peripheral blood and bone marrow, respectively. Considering the results of both the PCPI and BrdU assays, we used

a value of 3.5% of cells initiating proliferation over two days, giving a rate constant of 0.0175/day.

We also considered growth rate values from several mathematical models of tumor and immune cell interactions that are not specific to MM. Arciero et al. (2004) used a growth rate value of $r = 0.18$/day to represent growth of an aggressive tumor (doubling time of 3.85 days). de Pillis et al. (2005) used a tumor growth rate of 0.51/day based on mouse data from Diefenbach et al. (2001). Thus, we used a parameter range of 0.004-0.5/day for r_M.

Loss rate constant, δ_M: Hansen et al. (2014) estimated the half-life of M protein to be 11.9 days (equivalent to 0.058/day). Mills et al. (2017) cited the following half-life values for M protein: 21–25 days for an IgG subtype and 7–14 days for an IgA subtype (0.028-0.099/day). However, both of these studies were of patients who had received treatment that should contribute to the loss rate of M protein, so the cited half-lives are not due to δ_M alone. Moreover, in our equation for M, we also have several immune interactions contributing to loss of M, which we expect would be reflected in the half-lives cited above. Thus δ_M would be lower than if it were the only contribution to the half-lives cited above. If we assume Eq. (1) is in steady state, and if we use values shown in Table 2 for parameters other than δ_M, then we get a value between 0.001 and 0.002 for δ_M. We chose a range of 0.001-0.1/day for δ_M, and a value of 0.002.

Carrying capacity, K_M: Among 10,750 patients characterized in Greipp et al. (2005), the median M-protein level was 3.9 g/dL. A similar range was also observed in Tang et al. (2016) prior to treatment. Anecdotally, there are reports of values higher than 10 g/dL. We chose a range of 7–15 g/dL for the carrying capacity.

Growth and loss parameters for CTLs, T_C

Growth rate constant, r_C: de Boer et al. (2003) fit a differential equation model to data to characterize immune response during viral infection (lymphocytic choriomeningitis). They found that CD8+ cells have a biphasic response: an initial expansion phase with doubling time of 8 hours followed by a contraction phase with a half-life of 41 hours. The initial doubling time translates to a growth rate constant of $r_C \approx 2.31$/day. We used this number (for stimulated response) as an upper bound for r_C. A mathematical model of tumor and immune response by Arciero et al. (2004) used a sigmoidal dependence for effector cell proliferation, dependent on transforming growth factor beta (TGF-β) both for immune suppression and stimulation, with a maximum proliferation rate constant of 0.1245/day. de Pillis et al. (2013) estimated that IL-2 induces CD8+ T cell activation with a rate constant 1.11/day in a model of immune response for renal cell carcinoma. A mathematical model by de Boer et al. of T-lymphocyte anti-tumor response used a doubling time of 16 hours (1.04/day) for activated T cells (de Boer et al., 1985). We chose a parameter range of 0.01–0.5/day, which is slightly lower than the higher values cited above, as r_C reflects regular proliferation for CTL, with additional activation by myeloma and NK cells controlled by the parameters a_{MC}, b_{MC}, a_{NC}, and b_{NC}.

Carrying capacity, K_C: Using data presented in Pessoa de Magalhães et al. (2013), we estimated that CTL populations can reach levels as high as 1500 cells/μL in patients with MM, particularly in patients with long-term disease control. Thus, we chose 600–1500 cells/μL for the range of values considered for the carrying capacity K_C.

Loss rate constant, δ_C: Using a half-life value of 41 hours during a contraction phase of a viral infection as in de Boer et al. (2003), the loss rate constant would be 0.405/day. Sontag (2017) used a loss rate constant of 0.1/day. However, smaller rate constants have also been used. Arciero et al. (2004) gave a loss rate constant of 0.03/day for effector cells. de Boer et al. (1985) gave

a turnover time for T lymphocytes of 50 days (0.014/day). de Pillis et al. (2013) cited that CD8+ cells have a half-life of 77 days in healthy donors, which translates to a loss rate constant of 0.009/day (denoted by parameter m in their work). We thus considered a range of 0.01–0.5/day for δ_C.

Growth and loss parameters for NK cells, N

Constant source term, s_N: The source term s_N is included in our model because we expect the innate immune system to have non-negligible production of NK cells with efficacy against myeloma cells. de Pillis et al. (2005) used a constant source term of 1.3×10^4 cells/day for NK population dynamics. Dividing by a typical total blood volume of 5 liters for an adult, this results in 0.0026 cells/(μL·day). Zhang et al. (2007) gave a production rate of about 14×10^6 cells/(L · day) for healthy subjects and about 7×10^6 cells/(L·day) (7–14 cells/(μL·day)) for elderly subjects. We chose a parameter range of 0.001–5 cells/(μL·day).

Growth rate constant, r_N: An in vivo study of NK cells from healthy subjects found a doubling time of 16 days in healthy young adults (equivalent to 0.04/day), but a slower rate constant of 0.02/day (doubling time of 28 days) in healthy elderly subjects (Zhang et al., 2007). De Pillis et al. used a maximal rate constant of 0.5/day for NK cell recruitment by tumor cells (de Pillis et al., 2005), and another of their models gave a value of 0.0668/day for the maximum rate constant for NK cell proliferation induced by IL-2 (de Pillis et al., 2013). We chose a parameter range of 0.01–0.5/day for r_N.

Carrying capacity, K_N: Based on the higher range of observed NK cell levels of about 600 cells/μL among patients with MM (Pessoa de Magalhães et al., 2013), we chose a range of 300–650 cells/μL for the carrying capacity K_N.

Loss rate constant, δ_N: The in vivo studies of Zhang et al. (2007) gave half-lives of 10 or 11 days (mean for healthy elderly and healthy young adults, respectively), which translates to a loss rate constant of 0.06–0.07/day. The model in de Pillis et al. (2013) used a turnover rate constant of 0.0125/day for NK cells, and the model in de Pillis et al. (2005) used 0.0412/day. We chose a parameter range of 0.01–0.5/day.

Growth and loss parameters for Tregs, T_R

Growth rate constant, r_R: Vukmanovic-Stejic et al. (2006) assayed human samples and found that Tregs have a typical proliferation rate constant of 0.0831 cells/(μL·day). Similar to ranges we used for growth/loss rate constants for other immune cells, we considered a range of 0.01–0.5/day for r_R.

Carrying capacity, K_R: The high end of the range of Tregs reported in Pessoa de Magalhães et al. (2013) is about 100 cells/μL. We used a range of 60–120 cells/μL for K_R, and a value of 80 cells/μL.

Loss rate constant, δ_R: Vukmanovic-Stejic et al. (2006) also studied the turnover of Tregs. They found a turnover or loss rate constant of 0.0658/day. A mathematical model of tumor–immune interaction (Robertson-Tessi et al., 2012) used a loss rate constant of 0.1/day for the Treg population. We considered a range of 0.01–0.5/day, and a value of 0.757/day.

Saturating influence parameters

We allowed most of the a_{ij} values to vary from 0 to 10, i.e., from no change to more than an order of magnitude increase in size, depending on their function. We considered a slightly wider range for a_{NM}, a_{CM} and a_{CNM}, reflecting a high killing efficacy by immune cells. To ensure the correct sign for the loss rate for M, we needed $a_{MM} + a_{RM} \leq 1$. We allowed the threshold values, b_{ij}, to

vary between 0 to 2 times the respective carrying capacities. For point estimates of the b_{ij}, we chose values below half the respective carrying capacities.

Supplementary material

Supplementary material associated with this article, including code for the simulations and plots, can be found online at doi:10.1016/j.jtbi.2018.08.037.

References

Abbas, A.K., Lichtman, A.H., Pillai, S., 2015. Cellular and Molecular Immunology, Eighth Edition Elsevier Saunders, Philadelphia, PA.

Arciero, J., Jackson, T., Kirschner, D., 2004. A mathematical model of tumor-immune evasion and siRNA treatment. Discrete Continuous Dyn. Syst. Ser. B 4 (1), 39–58.

Balsa-Canto, E., Alonso, A.A., Banga, J., 2010. An iterative identification procedure for dynamic modeling of biochemical networks. BMC Syst. Biol. 4, 11.

de Boer, R.J., Hogeweg, P., Dullens, H.F., Weger, R.A.D., Otter, W.D., 1985. Macrophage T lymphocyte interactions in the anti-tumor immune response: a mathematical model. J. Immunol. 134 (4), 2748–2758.

de Boer, R.J., Homann, D., Perelson, A.S., 2003. Different dynamics of CD4+ and CD8+ T cell responses during and after acute lymphocytic choriomeningitis virus infection. J. Immunol. 171 (8), 3928–3935.

Boyman, O., Sprent, J., 2012. The role of interleukin-2 during homeostasis and activation of the immune system. Nat. Rev. Immunol. 12 (3), 180.

Brooks, S.P., 1998. Markov chain Monte Carlo method and its application. Statistician 47 (1), 69–100.

Brown, R., Pope, B., Yuen, E., Bibson, J., Joshua, D., 1998. The expression of T cell related costimulatory molecules in multiple myeloma. Leukemia Lymphoma 31 (3–4), 379–384.

Carbone, E., Neri, P., Mesuraca, M., Fulciniti, M.T., Otsuki, T., Pende, D., Groh, V., Spies, T., Pollio, G., Cosman, D., Catalano, L., Tassone, P., Rotoli, B., Venuta, S., 2005. HLA class I, NKG2D, and natural cytotoxicity receptors regulate multiple myeloma cell recognition by natural killer cells. Immunobiology 105 (1), 251–258.

Cerwenka, A., Baron, J., Lanier, L., 2001. Ectopic expression of retinoic acid early inducible-1 gene (RAE-1) permits natural killer cell-mediated rejection of a MHC class I-bearing tumor in vivo. Proc. Natl. Acad. Sci. 98 (20), 11521–11526.

Chen, M.-L., Pittet, M.J., Gorelik, L., Flavell, R.A., Weissleder, R., von Boehme, H., Khazaie, K., 2005. Regulatory T cells suppress tumor-specific CD8 T cell cytotoxicity through TGF-β signals in vivo. Proc. Natl. Acad. Sci. 102 (2), 419–424.

Chiş, O., Banga, J.R., Balsa-Canto, E., 2011. GenSSI: a software toolbox for structural identifiability analysis of biological models. Bioinformatics 27, 2610–2611.

D'Arena, G., Rossi, G., Laurenti, L., Statuto, T., D'Auria, F., Valvano, L., Simeon, V., Giudice, A., Innocenti, I., Feo, V.D., Filosa, R., Musto, P., 2016. Circulating regulatory T-cells in monoclonal gammopathies of uncertain significance and multiple myeloma: In search of a role. J. Immunol. Res. 2016. Article ID 9271469.

Dhodapkar, M.V., Geller, M.D., Chang, D.H., Shimizu, K., Fujii, S.-I., Dhodapkar, K.M., Krasovsky, J., 2003. A reversible defect in natural killer T cell function characterizes the progression of premalignant to malignant multiple myeloma. J. Exp. Med. 197 (12), 1667–1676.

Diefenbach, A., Jensen, E.R., Jamieson, A.M., Raulet, D.H., 2001. Rae1 and H60 ligands of the NKG2D receptor stimulate tumor immunity. Nature 413 (6852), 165.

Dimopoulos, M., Kyle, R., Fermand, J.-P., Rajkumar, S.V., Miguel, J.S., Chanan-Khan, A., Ludwig, H., Joshua, D., Mehta, J., Gertz, M., Avet-Loiseau, H., Beksaç, M., Anderson, K.C., Moreau, P., Singhal, S., Goldschmidt, H., Boccadoro, M., Kumar, S., Giralt, S., Munshi, N.C., behalf of the International Myeloma Workshop Consensus Panel 3, S.J., 2011. Consensus recommendations for standard investigative workup: report of the International Myeloma Workshop Consensus Panel 3. Blood 117 (18), 4701–4705.

DiPaolo, R.J., Glass, D.D., Bijwaard, K.E., Shevach, E.M., 2005. CD4+ CD25+ T cells prevent the development of organ-specific autoimmune disease by inhibiting the differentiation of autoreactive effector T cells. J. Immunol. 175 (11), 7135–7142.

d'Onofrio, A., 2005. A general framework for modelling tumor-immune system competition and immunotherapy: mathematical analysis and biomedical inferences. Physica D 208 (3–4), 220–235.

Dosani, T., Carlsten, M., Maric, I., Landgren, O., 2015. The cellular immune system in myelomagenesis: NK cells and T cells in the development of myeloma [corrected] and their uses in immunotherapies. Blood Cancer J. 5 (4), e306.

Durie, B.G., Salmon, S.E., 1975. A clinical staging system for multiple myeloma: correlation of measured myeloma cell mass with presenting clinical features, response to treatment, and survival. Cancer 36, 842–854.

Favaloro, J., Brown, R., Aklilu, E., Yang, S., Suen, H., Hart, D., Fromm, P., Gibson, J., Khoo, L., Ho, P.J., Joshua, D., 2014. Myeloma skews regulatory T and pro-inflammatory T helper 17 cell balance in favor of a suppressive state. Leukemia Lymphoma 55 (5), 1090–1098.

Feyler, S., von Lilienfeld-Toal, M., Jarmin, S., Marles, L., Rawstron, A., Ashcroft, A., Owen, R.G., Selby, P.J., Cook, G., 2009. CD4+CD25+FoxP3+ regulatory T cells are increased whilst CD3+CDCD8abTCR+ double negative T cells are decreased in the peripheral blood of patients with multiple myeloma which correlates with disease burden. Br. J. Haematol. 144, 686–695.

Feyler, S., Scott, G.B., Parrish, C., Jarmin, S., Evans, P., Short, M., McKinley, K., Selby, P.J., Cook, G., 2012. Tumour cell generation of inducible regulatory T-cells in multiple myeloma is contact-dependent and antigen-presenting cell-independent. PLoS ONE 7 (5), e35981.

Frohn, C., Hoppner, M., Schlenke, P., Kirchner, H., Koritke, P., Luhm, J., 2002. Anti-myeloma activity of natural killer lymphocytes. Br. J. Haematol. 119, 660–664.

Gallaher, J., Larripa, K., Ledzewicz, U., Renardy, M., Shtylla, B., Tania, N., White, D., Wood, K., Zhu, L., Passey, C., Robbins, M., Bezman, N., Shelat, S., Cho, H.J., Moore, H., 2018. A mathematical model for tumor-immune dynamics in multiple myeloma. Understanding Complex Biol. Syst. Math. To appear.

Gao, M., Gao, L., Yang, G., Tao, Y., Hou, J., Xu, H., Hu, X., Han, Y., Zhang, Q., Zhan, F., Wu, X., Shi, J., 2014. Myeloma cells resistance to NK cell lysis mainly involves an HLA class I-dependent mechanism. Acta Biochimica et Biophysica Sinica (Shanghai) 46 (7), 597–604.

Ghiringhelli, F., Ménard, C., Martin, F., Zitvogel, L., 2006. The role of regulatory T cells in the control of natural killer cells: relevance during tumor progression. Immunol. Rev. 214 (1), 229–238.

Ghiringhelli, F., Ménard, C., Terme, M., Flament, C., Taieb, J., Chaput, N., Puig, P.E., Novault, S., Escudier, B., Vivier, E., et al., 2005. CD4+ CD25+ regulatory T cells inhibit natural killer cell functions in a transforming growth factor-β-dependent manner. J. Exp. Med. 202 (8), 1075–1085.

van der Giessen, M., Rossouw, E., van Veen, T.A., van Loghem, E., Zegers, B., Sander, P., 1975. Quantification of IgG subclasses in sera of normal adults and healthy children between 4 and 12 years of age. Clin. Exp. Immunol. 21 (3), 501.

Golub, G.H., Van Loan, C.F., 2012. Matrix Computations, 3. Baltimore, MD: The Johns Hopkins University Press.

Gonzalez-Qunitela, A., Alende, R., Gude, F., Campos, J., Rey, J., Meijide, L., 2008. Serum levels of immunoglobulins (igg, iga, igm) in a general adult population and their relationship with alcohol consumption, smoking and common metabolic abnormalities. Clin. Exp. Immunol. 151 (5), 42–50.

Greipp, P.R., Miguel, J.S., Durie, B.G., Crowley, J.J., Barlogie, B., Bladé, J., Boccadoro, M., Child, J.A., Avet-Loiseau, H., Kyle, R.A., Lahuerta, J.J., Ludwig, H., Morgan, G., Powles, R., Shimizu, K., Shustik, C., Sonneveld, P., Tosi, P., Turesson, I., Westin, J., 2005. International staging system for multiple myeloma. J. Clin. Oncol. 23 (15), 3412–3420.

Hansen, C.T., Pedersen, P.T., Nielsen, L.C., Abildgaard, N., 2014. Evaluation of the serum free light chain (sFLC) analysis in prediction of response in symptomatic multiple myeloma patients: Rapid profound reduction in involved FLC predicts achievement of VGPR. Eur. J. Haematol. 93 (5), 407–413.

Hastings, W.K., 1970. Monte Carlo sampling methods using Markov chains and their applications. Biometrika 57 (1), 97–109.

Hokanson, J.A., Brown, B.W., Thompson, J.R., Drewinko, B., Alexanian, R., 1977. Tumor growth patterns in multiple myeloma. Cancer 39, 1077–1084.

Iman, R.L., 2008. Latin hypercube sampling. In: Melnick, E.L., Everitt, B.S. (Eds.), Encyclopedia of Quantitative Risk Analysis and Assessment, 1. Wiley Online Library.

Ingalls, B.P., 2013. Mathematical Modeling in Systems Biology: An Introduction. Cambridge, MA: MIT Press.

Janeway, C.A., 2001. How the immune system protects the host from infection. Microbes Infect. 3 (13), 1167–1171.

Jonsson, F., Ou, Y., Claret, L., Siegel, D., Jagannath, S., Vij, R., Badros, A., Aggarwal, S., Bruno, R., 2015. A tumor growth inhibition model based on M-protein levels in subjects with relapsed/refractory multiple myeloma following single-agent carfilzomib use. CPT Pharmacometrics Syst. Pharmacol. 4 (12), 711–719.

Kawano, Y., Moschetta, M., Manier, S., Glavey, S., Görgün, G.T., Roccaro, A.M., Anderson, K.C., Ghobrial, I.M., 2015. Targeting the bone marrow microenvironment in multiple myeloma. Immunol. Rev. 263 (1), 160–172.

Kawarada, Y., Ganss, R., Garbi, N., Sacher, T., Arnold, B., Hämmerling, G.J., 2001. NK- and CD8+ T cell-mediated eradication of established tumors by peritumoral injection of CpG-containing oligodeoxynucleotides. J. Immunol. 167 (9), 5247–5253.

Kazandjian, D., Landgren, O., 2016. A look backward and forward in the regulatory and treatment history of multiple myeloma: approval of novel-novel agents, new drug development, and longer patient survival. Semin. Oncol. 43, 682–689.

Kendall, M.G., 1942. Partial rank correlation. Biometrika 32 (3/4), 277–283.

Kim, J.M., Rasmussen, J.P., Rudensky, A.Y., 2007. Regulatory T cells prevent catastrophic autoimmunity throughout the lifespan of mice. Nat. Immunol. 8 (2), 191–197.

Kirschner, D., Panetta, J.C., 1998. Modeling immunotherapy of the tumor-immune interaction. J. Math. Biol. 37, 235–252.

Kumar, S., Rajkumar, S.V., Greipp, P.R., Witzig, T.E., 2004. Cell proliferation of myeloma plasma cells: comparison of the blood and marrow compartments. Pharmaceuticals (Basel) 77, 7–11.

Kuznetsov, V.A., Makalkin, I.A., Taylor, M.A., Perelson, A.S., 1994. Nonlinear dynamics of immunogenic tumors: parameter estimation and global bifurcation analysis. Bull. Math. Biol. 56 (2), 295–321.

Kyle, R.A., Gertz, M.A., Witzig, T.E., Lust, J.A., Lacy, M.Q., Dispenzieri, A., Fonseca, R., Rajkumar, S.V., Offord, J.R., Larson, D.R., et al., 2003. Review of 1027 patients with newly diagnosed multiple myeloma. In: Mayo Clinic Proceedings, 78. Elsevier, pp. 21–33.

Kyle, R.A., Isbaudi, F., Rajkumar, S.V., 2011. Management of monoclonal gammopathy of undetermined significance (MGUS) and smoldering multiple myeloma (SMM). Oncology (Williston Park) 25 (7), 578–586.

Lehman, C., Zeis, M., Uharek, L., 2001. Activation of natural killer cells with interleukin 2 (IL-2) and IL-12 increases perforin binding and subsequent lysis of tumour cells. Br. J. Haematol. 114 (3), 660–665.

Marino, S., Hogue, I.B., Ray, C.J., Kirschner, D.E., 2008. A methodology for performing global uncertainty and sensitivity analysis in systems biology. J. Theor. Biol. 254, 178–196.

Mempel, T.R., Pittet, M.J., Khazaie, K., Weninger, W., Weissleder, R., von Boehmer, H., von Andrian, U.H., 2006. Regulatory T cells reversibly suppress cytotoxic T cell function independent of effector differentiation. Immunity 25 (1), 129–141.

Meropol, N.J., Barresi, G.M., Fehniger, T.A., Hitt, J., Franklin, M., Caligiuri, M.A., 1998. Evaluation of natural killer cell expansion and activation in vivo with daily sub-cutaneous low-dose interleukin-2 plus periodic intermediate-dose pulsing. Cancer Immunol. Immunother. 46 (6), 318–326.

Mills, J., Barnidge, D., Dispenzieri, A., Murray, D., 2017. High sensitivity blood-based M-protein detection in sCR patients with multiple myeloma. Blood Cancer J. 7 (8), e590.

Moore, H., Li, N.K., 2004. A mathematical model for chronic myelogenous leukemia (CML) and T cell interaction. J. Theor. Biol. 227 (4), 513–523.

Nanavati, C., Ruszaj, D., Mager, D.E., 2017. Cell signaling model connects vorinostat pharmacokinetics and tumor growth response in multiple myeloma xenografts. CPT Pharmacometrics Syst. Pharmacol. 6, 756–764.

Nardiello, T., Jungbluth, A.A., Mei, A., DiLiberto, M., Huang, X., Dabrowski, A., An-drade, V.C., Wasserstrum, R., Ely, S., Niesvizky, R., Pearse, R., Coleman, M., Jaya-balan, D.S., Bhardwaj, N., Old, L.J., Chen-Kiang, S., Cho, H.J., 2011. MAGE-A in-hibits apoptosis in proliferating myeloma cells through repression of Bax and maintenance of survivin. Clin. Cancer Res. 17 (13), 4309–4319.

Olufsen, M.S., Ottesen, J.T., 2013. A practical approach to parameter estimation ap-plied to model predicting heart rate regulation. J. Math. Biol. 67 (1), 39–68.

Pallmer, K., Oxenius, A., 2016. Recognition and regulation of T cells by NK cells. Front. Immunol. 7, 215. doi:10.3389/fimmu.2016.00251.

Pessoa de Magalhães, R.J., Vidriales, M.-B., Paiva, B., Fernandez-Gimenez, C., García-Sanz, R., Mateos, M.-V., Gutierrez, N.C., Lecrevisse, Q., Blanco, J.F., Hernández, J., de las Heras, N., Martinez-Lopez, J., Roig, M., Costa, E.S., Ocio, E.M., Perez-Andres, M., Maiolino, A., Nucci, M., Rubia, J.D.L., Lahuerta, J.-J., San-Miguel, J.F., Orfao, A., 2013. Analysis of the immune system of multiple myeloma pa-tients achieving long-term disease control by multidimensional flow cytometry. Haematologica 98 (1), 79–86. doi:10.3324/haematol.2012.067272.

de Pillis, L., Caldwell, T., Sarapata, E., Williams, H., 2013. Mathematical modeling of regulatory T cell effects on renal cell carcinoma treatment. Discrete Continuous Dyn. Syst. Ser. B 18 (4), 915–943.

de Pillis, L.G., Radunskaya, A., Wiseman, C.L., 2005. A validated mathematical model of cell-mediated immune response to tumor growth. Cancer Res. 65, 7950–7958.

Plebani, A., Ugazio, A., Avanzini, M., Massimi, P., Zonta, L., Monafo, V., Burgio, G., 1989. Serum IgG subclass concentrations in healthy subjects at different age: age normal percentile charts. Eur. J. Pediatr. 149 (3), 164–167.

Pope, S.R., Ellwein, L.M., Zapata, C.L., Novak, V., Kelley, C.T., Olufsen, M.S., 2009. Es-timation and identification of parameters in a lumped cerebrovascular model. Math. Biosci. Eng. 6 (1), 93–115.

Pratt, G., Goodyear, O., Moss, P., 2007. Immunodeficiency and immunotherapy in multiple myeloma. Br. J. Haematol. 138 (5), 563–579.

Raitakari, M., Brown, R., Gibson, J., Joshua, D., 2003. T cells in myeloma. Hematol. Oncol. 21 (1), 33–42.

Raja, K.R.M., Rihova, L., Zahradova, L., Klincova, M., Penka, M., Hajek, R., 2012. In-creased t regulatory cells are associated with adverse clinical features and pre-dict progression in multiple myeloma. PLoS ONE 7 (10), e47077.

Robertson-Tessi, M., El-Kareh, A., Goriely, A., 2012. A mathematical model of tu-mor-immune interactions. J. Theor. Biol. 294, 56–73.

Salmon, S.E., Smith, B.A., 1970. Immunoglobulin synthesis and total body tumor cell number in IgG multiple myeloma. J. Clin. Invest. 49, 1114–1121.

Shanker, A., Buferne, M., Schmitt-Verhulst, A.-M., 2010. Cooperative action of CD8 T lymphocytes and natural killer cells controls tumour growth under conditions of restricted T-cell receptor diversity. Immunology 129 (1), 41–54.

Shanker, A., Verdeil, G., Buferne, M., Inderberg-Suso, E.-M., Puthier, D., Joly, F., Nguyen, C., Leserman, L., Auphan-Anezin, N., Schmitt-Verhulst, A.-M., 2007. CD8 T cell help for innate antitumor immunity. J. Immunol. 179 (10), 6651–6662.

Shevach, E.M., DiPaolo, R.A., Andersson, J., Zhao, D.-M., Stephens, G.L., Thorn-ton, A.M., 2006. The lifestyle of naturally occurring CD4+ CD25+ Foxp3+ reg-ulatory T cells. Immunol. Rev. 212 (1), 60–73.

Shook, D.R., Campana, D., 2011. Natural killer cell engineering for cellular therapy of cancer. Tissue Antigens 78 (6), 409–415.

Smyth, M.J., Teng, M.W., Swann, J., Kyparissoudis, K., Godfrey, D.I., Hayakawa, Y., 2006. CD4+ CD25+ T regulatory cells suppress NK cell-mediated immunother-apy of cancer. J. Immunol. 176 (3), 1582–1587.

Sontag, E.D., 2017. A dynamic model of immune responses to antigen presentation predicts different regions of tumor or pathogen elimination. Cell. Syst. 4 (2), 231–241.

Stepanova, N., 1980. Course of the immune reaction during the development of a malignant tumour. Biophysics 24, 917–923.

Stoop, J., Zegers, B., Sander, P., Ballieux, R., 1969. Serum immunoglobulin levels in healthy children and adults. Clin. Exp. Immunol. 4 (1), 101.

Suen, H., Brown, R., Yang, S., Weatherburn, C., Ho, P., Woodland, N., Nassif, N., Bar-baro, P., Bryant, C., Hart, D., et al., 2016. Multiple myeloma causes clonal T–cell immunosenescence: identification of potential novel targets for promoting tumour immunity and implications for checkpoint blockade. Leukemia 30 (8), 1716–1724.

Sullivan, P.W., Salmon, S.E., 1972. Kinetics of tumor growth and regression in IgG multiple myeloma. J. Clin. Invest. 51, 1697–1708.

Sungur, C.M., Tang-Feldman, Y.J., Ames, E., Alvarez, M., Chen, M., Longo, D.L., Pomeroy, C., Murphy, W.J., 2013. Murine natural killer cell licensing and reg-ulation by T regulatory cells in viral responses. Proc. Natl. Acad. Sci. 110 (18), 7401–7406.

Swan, G.W., Vincent, T.L., 1977. Optimal control analysis in the chemotherapy of IgG multiple myeloma. Bull. Math. Biol. 39 (3), 317–337. doi:10.1016/S0092-8240(77)80070-0.

Tang, M., Zhao, R., van de Velde, H., Tross, J.G., Mitsiades, C., Viselli, S., Neuwirth, R., Esseltine, D.-L., Anderson, K., Ghobrial, I.M., Miguel, J.F.S., Richardson, P.G., Tomasson, M.H., Michor, F., 2016. Myeloma cell dynamics in response to treat-ment supports a model of hierarchical differentiation and clonal evolution. Clin. Cancer Res. 22 (16), 4206–4214. doi:10.1158/1078-0432.CCR-15-2793.

Tran, D.Q., 2012. TGF-β: the sword, the wand, and the shield of FOXP3+ regulatory T cells. J Mol Cell Biol 4 (1), 29–37.

de Vladar, H.P., González, J.A., 2004. Dynamic response of cancer under the influ-ence of immunological activity and therapy. J. Theor. Biol. 227 (3), 335–348.

Vukmanovic-Stejic, M., Zhang, Y., Cook, J.E., Fletcher, J.M., McQuaid, A., Masters, J.E., Rustin, M.H., Taams, L.S., Beverley, P.C., Macallan, D.C., et al., 2006. Human CD4+ CD25hi Foxp3+ regulatory T cells are derived by rapid turnover of memory pop-ulations in vivo. J. Clin. Invest. 116 (9). 24–23.

Wen, Y.-J., Min, R., Tricot, G., Barlogie, B., Yi, Q., 2002. Tumor lysate-specific cytotoxic t lymphocytes in multiple myeloma: promising effector cells for immunother-apy. Blood 99 (9), 3280–3285.

Zhang, Y., Wallace, D.L., Lara, C.M.D., Ghattas, H., Asquith, B., Worth, A., Griffin, G.E., Taylor, G.P., Tough, D.F., Beverley, P.C., Macallan, D.C., 2007. In vivo kinetics of human natural killer cells: the effects of ageing and acute and chronic viral infection. Immunology 121 (2), 258–265.